Katharina Kocher, BSc.

Functionalized catalysts for the oxygen reduction reaction toward durable high temperature PEM fuel cells

MASTER'S THESIS

to achieve the university degree of

Diplom-Ingenieurin

Master's degree programme: Technical Chemistry

submitted to

Graz University of Technology

Supervisors

Assoc. Prof. DI Dr. Viktor Hacker

DI Dr. Alexander Schenk, BSc.

Institute of Chemical Engineering and Environmental Technology

Graz University of Technology

Graz, March 2017

Affidavit

I declare that I have authored this thesis independently, that I have not used other than the declared sources/resources, and that I have explicitly marked all material, which has been quoted either literally or by content from the sources used. The text document uploaded on TUGRAZonline is identically to the present master's thesis.

Ich erkläre an Eides statt, dass ich die vorliegende Arbeit selbstständig verfasst, andere als die angegebenen Quellen/Hilfsmittel nicht benutzt, und die den benutzten Quellen wörtlich und inhaltlich entnommenen Stellen als solche kenntlich gemacht habe. Das in TUGRAZonline hochgeladene Textdokument ist mit der vorliegenden Masterarbeit identisch.

…… ……

Date Signature

Acknowledgements

At this point I would like to thank all those, who accompanied and motivated me during the preparation of this master thesis.

First of all, I would like to thank my supervisor Assoc. Prof. Viktor Hacker for the opportunity to write this master thesis and thank for his support during this time. His competent advice and help came to my advantage in many matters.

Special thanks go to DI Dr. Alexander Schenk, who gave me extraordinary expert, experienced and valuable support in the planning, implementation and evaluation of this work at any time. I am very grateful for his dedicated encouragement and creative ideas. Moreover, many thanks go of course to the entire fuel cell working group for their friendliness, help and guidance throughout my time at the Institute of Chemical Engineering and Environmental Technology. The collaborations and events with you were great and enriching experiences that I would not want to miss.

Last, but not least, I would like to thank Florian for his strong and constant emotional support. I wish to express my deepest gratitude to him for motivating me in difficult times and his understanding.

Finally, I would like to thank my family, and especially my parents, who have made my studies possible through their moral and financial support, and for providing me with all the help I needed.

Kurzfassung

Da aktuell keine flächendeckende Wasserstoffinfrastruktur existiert, wird an Brennstoffzellentypen geforscht, die mit reformierten Kohlenwasserstoffen betrieben werden können. Diesbezüglich ist die Hochtemperatur-Polymerelektrolytmembran (HT-PEM) Brennstoffzelle eine vielversprechende Technologie für die dezentrale Bereitstellung von Energie. In diesen elektrochemischen Energieumwandlungssystemen werden mit Phosphorsäure (PA) dotierte Polymermembranen als Elektrolyt verwendet. Gegenüber herkömmlichen flüssigen Elektrolyten sind diese einfach in der Handhabung und besitzen exzellente Eigenschaften. Die hohe Ionenleitfähigkeit der Membran wird durch Wechselwirkung zwischen Polymer und PA beeinflusst. Allerdings limitiert die Anwesenheit von PA signifikant die katalytische Leistung der Platinkatalysatoren gegenüber der Sauerstoffreduktionsreaktion (ORR), da Phosphatspezies an der Katalysatoroberfläche adsorbieren und somit zu einer Reduktion der katalytisch aktiven Fläche bzw. Aktivität führen.

Anfänglich wurde die vergiftende Wirkung der PA auf einen kohlenstoffgeträgerten Platinkatalysator (Pt/C) untersucht. Um die resultierende Leistungsverschlechterung zu verringern wurden neu synthetisierte Katalysatoren in der Anwesenheit von PA getestet. Diese neuen Katalysatoren basieren auf einer Funktionalisierung mit Polyanilin (PANI). PANI bildet einen schützenden dünnen Film um die Katalysatorpartikel und unterbindet somit die Adsorption der PA auf der Katalysatoroberfläche, ohne dabei negativ die katalytische Aktivität zu beeinflussen. In diesem Zusammenhang wurden PANI-dekorierte Platinkatalysatoren (Pt/C@PANI) und Platinkobaltkatalysatoren (Pt-Co/C@PANI) durch oxidative Polymerisation von Anilin synthetisiert. Die elektrochemische ex-situ Charakterisierung erfolgte mittels Rotating Disk Electrode.

Die Ergebnisse aus den zyklischen Voltammetrie- und ORR-Experimenten ergaben, dass die katalytische Aktivität stark vom PANI-Gehalt abhängt. Trotzdem zeigen Pt/C@PANI und Pt-Co/C@PANI eine signifikante Stabilität gegenüber der PA, was zu einem geringeren Verlust der elektrochemisch aktiven Oberfläche führt. Darüber hinaus besitzen diese Katalysatoren eine hohe Massenaktivität und spezifische Stromdichten im Vergleich zu herkömmlichen Pt/C Katalysatoren.

Abstract

As a widespread hydrogen infrastructure is currently not existing, research is focused on fuel cell (FC) types that can operate directly with reformed hydrocarbons. Referring to this, high temperature polymer electrolyte membrane (HT-PEM) FCs represent promising candidates for a widespread decentralized energy supply. These electrochemical energy conversion devices use polymer membranes doped with phosphoric acid (PA). Compared to conventional liquid electrolytes these membranes are simple to handle and provide excellent properties for FC application. The high ion conductivity of the membrane is influenced by the interaction between the polymer and the PA. However, the presence of PA significantly limits the performance of the platinum (Pt) catalyst toward the oxygen reduction reaction (ORR). This is attributed to the coverage of the Pt surface by several phosphate species, which leads to a reduction of the catalyst's active sites and activity.

Initially the poisoning effect of PA on a carbon supported Pt catalyst (Pt/C) was investigated. In order to mitigate performance losses of the Pt/C catalyst in PA environment, newly synthesized electrocatalysts were tested. The new catalysts are based on a functionalization with polyaniline (PANI). PANI is known to form a protecting thin film around the catalyst particles, and thus inhibits the surface coverage of the catalyst by PA without sacrificing its activity.

In this context, PANI decorated Pt/C catalysts (Pt/C@PANI) and platinum cobalt catalysts (Pt-Co/C@PANI) were synthesized through oxidative polymerization of aniline. Electrochemical ex-situ characterization was performed by means of thin film rotating disk electrode technique.

The results of cyclic voltammetry and ORR experiments revealed that the catalytic activity of these catalysts depends on the content of PANI. Nevertheless, Pt/C@PANI and Pt-Co/C@PANI exhibit significantly higher stability toward the PA, resulting in less loss of the electrochemical surface area. Moreover, they demonstrate higher mass activity and specific current density compared with that of the undecorated Pt/C catalysts.

Abbreviations

APS	Ammonium persulfate
CHP	Combined heat and power unit
CE	Counter electrode
CL	Catalyst layer
CV	Cyclic voltammetry
ECSA	Electrochemical active surface area
Eq.	Equation
FC	Fuel cell
GDL	Gas diffusion layer
GDM	Gas diffusion media
GHG	Greenhouse gas
HHV	Higher heating value
HOMO	Highest occupied molecular orbital
HOR	Hydrogen oxidation reaction
HR	High resolution
HSAC	High surface area carbon
HT	High temperature
H_{upd}	Hydrogen underpotentially deposited
LHV	Lower heating value
LUMO	Lowest unoccupied molecular orbital
LT	Low temperature
MA	Mass activity
MEA	Membrane electrode assembly
MPL	Microporous layer

OCV	Open circuit voltage
ORR	Oxygen reduction reaction
PA	Phosphoric acid
PANI	Polyaniline
PBI	Polybenzimidazole
PEM	Polymer electrolyte membrane
PEMFC	Polymer electrolyte membrane fuel cell
PFSA	Perfluorosulfonic acid polymer
PTFA	Polytetrafluoroethylene
Pt	Platinum
Pt/C	Carbon supported platinum catalyst
Pt/C@PANI	Carbon supported PANI decorated platinum catalyst
Pt-Co/C	Carbon supported platinum cobalt catalyst
Pt-Co/C@PANI	Carbon supported PANI decorated platinum cobalt catalyst
RDE	Rotating disk electrode
RHE	Reference hydrogen electrode
SCD	Specific current density
TEM	Transmission electron microscopy
WE	Working electrode

Content

1 Introduction

The combustion of fossil resources, like coal, oil and natural gas, will continue to dominate the global power generation. Thereby, the concentration of greenhouse gas (GHG) emissions in the atmosphere, which are mainly associated with CO_2, will significantly increase. Consequently, these severe GHGs lead to an increase of the globe's surface temperature, known as global warming (see Figure 1) [1].

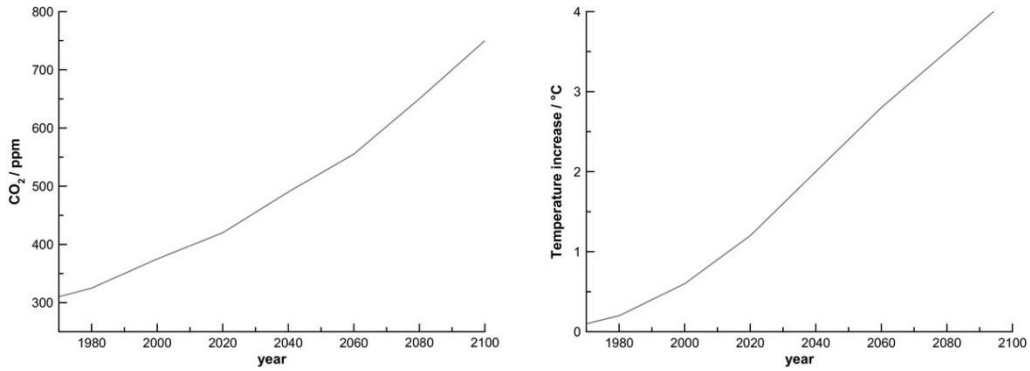

Figure 1 Long term increasing CO_2 emissions (left) effecting global warming (right) [3]

In 2015, at the 21st Conference of the Parties (COP21) in Paris, a framework on climate change was achieved. This agreement targets the aim to keep global warming below 2 °C and to reduce GHG emissions significantly [2]. The awareness of environmental concerns as well as the dependency on limited conventional energy sources heightened interest in the development of renewable technologies for a secure and sustainable energy generation. With respect to the intermittent and fluctuating nature of several renewable resources (solar, wind, etc.), which have been increasingly implemented in the last few years, advanced energy conversion and storage technologies are needed to provide a continuous supply of energy [3].

In this way, hydrogen (H_2) and fuel cells (FC) are considered to generate clean energy in the future. Since H_2, which is the most abundant element on Earth's surface, has the highest energy content of all fuels, it becomes a potential candidate for energy storage and distribution. As of now, 95% of H_2 are produced by natural gas reforming or from gasification of coal [4]. Also, renewable biofuels may be converted to H_2 using different chemical conversion technologies. Power-to-gas offers another way to produce H_2 by water electrolysis.

Moreover, beside its storage either in compressed or liquefied form, the approach of using chemical hydrogen carriers has been developed [5].

FCs are one of the most versatile devices reconverting stored H_2 energy. They combine H_2 and oxygen (O_2) to produce electric energy, water and heat highly efficient and almost emission free. Unlike batteries, the benefit of FCs is that they do not require any recharging and produce electricity as long as the reactants are supplied. Nowadays, FCs are being actively used in transport applications (cars, busses, etc.) as well as for a wide range of portable applications. Furthermore, they are applied in residentially combined heat and power (CHP) systems enabling distributed electricity and heat generation [5]. Depending on the application, energy scale, operation temperature or electrolyte different types of FCs have been developed.

Among them, high temperature polymer electrolyte membrane (HT-PEM) FCs gained much interest because they provide a high tolerance toward impurities. Usually, the H_2 originating from reformed hydrocarbons contains poisoning carbon monoxide (CO). Due to the elevated operation temperatures of HT-PEM FCs it is possible to use the fuel directly without previous purification and without sacrificing the overall performance [6]. Nevertheless, one drawback of such high temperature FC systems cannot be mitigated. They use phosphoric acid (H_3PO_4, PA) in their electrolyte. As a result, phosphate species adsorb on the surface of the platinum (Pt) catalyst and affect negatively the kinetics of the oxygen reduction reaction (ORR), which proceeds at the cathode [7]. As the ORR limits the overall cell performance new techniques to inhibit the negative influence of H_3PO_4 gained importance on the way of FCs becoming economically viable within their lifetime and efficiency.

In this context, the driving force of the present work was the preparation of modified Pt based catalysts for the cathode side in HT-PEM FCs in order to minimize phosphates adsorption and to provide advanced catalytic performances including ORR activity and stability. This study takes advantage of the “third-body-effect” [8]. There, small amounts of an organic molecule are pre-adsorbed on the catalyst surface in order to inhibit phosphates adsorption. Polyaniline (PANI) groups are known to interact with PA when they are attached to the catalyst. So, PA species may not occlude the Pt catalyst’s active sites [9]. For the purpose to achieve the mentioned requirements, a commercial Pt catalyst and a commercial Pt cobalt catalyst are functionalized with PANI (Pt/C@PANI, Pt-Co/C@PANI) and are compared to in-house

synthesized equivalents. Using these newly fabricated electrocatalysts opens the possibility to improve the catalytic performance by reducing phosphates adsorption.

2 Theory

2.1 Fuel cell basics

A FC is an electrochemical device producing electricity, heat and water by merging a gaseous fuel (H_2) and an oxidant gas (O_2).

As any electrochemical cell, FCs are built up of an electrolyte and two electrodes (anode and cathode). In general, the electrolyte must afford high ionic conductivity, high thermal and high chemical stability. The electrodes, which have a porous structure, enabling the gases to arrive at the reaction site, have to provide high electric conductivity [10]. The basic scheme of a FC, in this case of a polymer electrolyte membrane (PEM) FC, is illustrated in Figure 2.

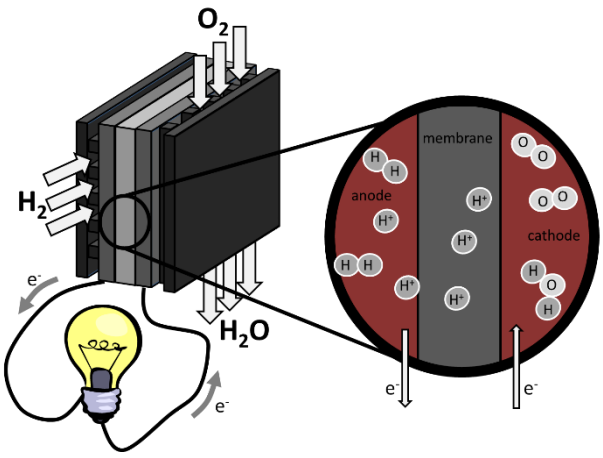

Figure 2 Principle of a PEM FC, adopted from [11]

Considering various types of FCs, PEM FCs are as the most promising type, due to their numerous benefits, including high efficiency, high power densities, fast start up and long stack life. They provide the perfect basis for a low, almost non-pollutant alternative to our current energy system [12] .

The central component of a PEM FC is the so-called membrane electrode assembly, abbreviated as MEA. It consists of a membrane electrolyte, which is a solid polymeric film, sandwiched between two porous electrodes. Compared to liquid electrolytes, the handling of these thin and elastic membrane electrolytes in the assembly is simplified. The PEM is designed as electric insulator material with high ion conductivity in order to allow only protons

to move toward the electrodes. Moreover, it separates the compartments and provides excellent resistance to gas permeation to avoid the mixing of H_2 and O_2. In order to meet a long durability, the membrane should offer high chemical, mechanical and thermal stability in the fuel cell environment [13]. Most practically, fluorosulfonated ionomers (perfluorosulfonic acid, PFSA) are employed, whereby the polytetrafluoroethylene (Teflon)-like backbone grants good mechanical and thermal stability. The super acid sulfonic acid groups (-SO_3H) provide the necessary proton conductivity and the side chains (-O-CF_2-CF-O-CF_2-CF_2-) connect the backbone with the -SO_3H groups [12]. To maintain a high proton conductivity of about 0.1 S cm^{-1}, these membranes must be well hydrated. Usually, to solve this problem the air, the H_2 or both are humidified before they enter the cell [5].

The porous structure of the electrodes facilitates the gas transport to the active layer. Therefore, each electrode is composed of a catalyst layer (CL) and a gas diffusion layer (GDL). Latter consists of a gas diffusion media (GDM) made out of a carbon gas diffusion paper and the microporous layer (MPL). Usually, high surface area carbon (HSAC), which provides a fine structured porous network and PTFE, which renders the GDL hydrophobic, build up the MPL. The CL contains an active catalyst, mainly Pt supported on HSAC to perform the oxidation of H_2 at the anode (hydrogen oxidation reaction, HOR) and the reduction of O_2 on the cathode (oxygen reduction reaction, ORR) [12].

Electrochemical energy converters operate by means of separate “cold combustion”. This means that FCs are able to convert the internal energy of a fuel directly into electrical energy and heat via separate electrode reactions. Thus, this leads to higher conversion efficiencies compared to conventional internal combustion engines. In other words, FCs produce more electricity from the same amount of fuel than other combustion technologies [14].

The reactions, which occur between H_2 and O_2 are summarized below (Eq. 1, Eq. 2 and Eq. 3).

Anode reaction (HOR)	$\mathrm{H_2} \leftrightarrow 2\mathrm{H^+} + 2\mathrm{e^-}$	Eq. 1
Cathode reaction (ORR)	$\frac{1}{2}\mathrm{O_2} + 2\mathrm{H^+} + 2\mathrm{e^-} \leftrightarrow \mathrm{H_2O}$	Eq. 2
Overall reaction	$\mathrm{H_2} + \frac{1}{2}\mathrm{O_2} \leftrightarrow \mathrm{H_2O}$	Eq. 3

H_2 is fed to the anode, where it adsorbs on the catalyst surface and gets oxidized. Thereby it releases electrons (e^-) and forms protons (H^+) through the HOR. The electrons flow through the GDL and are collected in an external circuit, producing electrical energy. The protons are capable to diffuse through the PEM to the cathode, where they react with O_2 and electrons forming water (H_2O) via the ORR [15] .

For a reversible system the maximum generated electrical work is related to the Gibbs free energy ΔG [16].

$$\Delta G^0 = -nFE_{th} \qquad \text{Eq. 4}$$

with ΔG^0 the molar specific Gibbs free energy of liquid water (ΔG^0=-273.34 kJ mol^{-1}), n the number of electrons and F the Faraday constant (96485 C mol^{-1}).

Thus, Eq. 5 gives the theoretical cell voltage E_{th} of a H_2/O_2 FC at 25 °C and 1 atm, assuming that the product is liquid water.

$$E_{th} = -\frac{\Delta G^0}{nF} = 1.23\ V \qquad \text{Eq. 5}$$

However, the real cell voltage E_{cell} and thus the performance is affected by several voltage losses as the cell is connected to an electrical load (see Figure 3) [10].

$$E_{cell} = E_{rev} - \Delta E_{ohm} - \eta_{ORR} - \eta_{mt} \qquad \text{Eq. 6}$$

E_{rev} describes the reduced open circuit voltage (OCV) at real reaction conditions considering pressure and temperature of the reactants. E_{ohm} results from occurring ohmic resistances within the cell. η_{mt} considers mass transport losses due to the slow transport of O_2 to the cathode and losses due to the sluggish kinetics of the ORR are given by η_{ORR} [17].

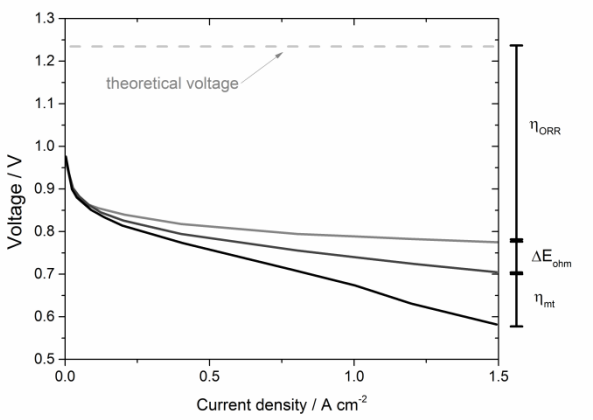

Figure 3 Influence of voltage losses on E_{real}. Figure adapted from [11]

The theoretical (maximum possible) efficiency η_{ideal} of a PEM FC is given by the ratio of maximum energy output based on the free Gibbs energy ΔG and the energy input based on the enthalpy ΔH.

$$\eta_{ideal} = \frac{\Delta G}{\Delta H_{HHV}} = 0.83 \qquad \text{Eq. 7}$$

If liquid water is produced the higher heating value (HHV) (ΔH^0_{HHV} = 285.6 kJ mol^{-1}) defines the reaction enthalpy, when gaseous water is produced the lower heating value (LHV) (ΔH^0_{LHV} = 241.2 kJ mol^{-1}) defines the reaction enthalpy [12]. From the equation above (Eq. 7) the theoretical efficiency results in a value of 83% based on the HHV of H_2.

The real efficiency η_{real} of an operated FC can be given by Eq. 8 and ranges from 50-70% for PEM FCs.

$$\eta_{real} = \frac{E}{E_{rev}} \qquad \text{Eq. 8}$$

2.2 High temperature PEM fuel cells

In recent years, the operation of PEM FCs at elevated temperatures has been recognized as a promising solution to overcome limitations of low temperature (LT-) PEM FCs. Relative to LT-PEM FCs, which are operated at 80 °C, HT-PEM FCs work in a range from 100 °C to 200 °C.

The main advantages of using HT-PEM FCs include a better tolerance toward impurities, enhanced reaction kinetics as well as a simplified heat and water management [18].

2.2.1 Benefits of HT-PEM FCs

2.2.1.1 Improved tolerance to impurities

As mentioned above, usually the supplied fuels contain undesired impurities. The oxidant (air) consists of contaminants from industry, traffic and agriculture. As the H_2 gas comes mainly from steam reforming, it contains a considerable amount of CO, which is one of the main contaminants for FCs. Since CO has a high affinity to Pt surfaces it is a poison for Pt and Pt based catalysts. The increasing coverage of CO on the Pt surface leads to a decrease in the overall performance of a FC. It is assumed that this adsorption of CO is favored at low temperatures. The tolerance towards CO increases dramatically with the temperature [6]. For HT-PEM FCs the tolerance increases up to 3% by volume in the anode gas stream [19]. In contrast to HT-PEM FCs, which can use the H_2 gas directly, it is necessary to purify the fuel before it is applied in LT-PEM FCs.

2.2.1.2 Enhanced cathode kinetics

Considering the occurring half-cell reactions in FCs, the HOR is much faster ($i^0_{H2} = 10^{-4}$ - 10^{-3} A m^{-2}) than the ORR ($i^0_{O2} = 10^{-9}$ - 10^{-8} A cm^{-2}), which therefore limits the overall kinetics [18]. The reaction rate of any chemical reaction is limited by an activation energy (E_a). Before the reactants are converted into the products they have to overcome this energy barrier (see Figure 4). The lower E_a the easier it is for the reactants to react to the products. In the case of FCs, a charge must overcome this barrier to move from the electrode through the electrolyte and vice versa. The main ways of dealing with the slow reaction rates of the ORR are the use of a catalyst, the increase of the electrode areas as well as the elevation of the operation temperature, as in HT-PEM FCs [5].

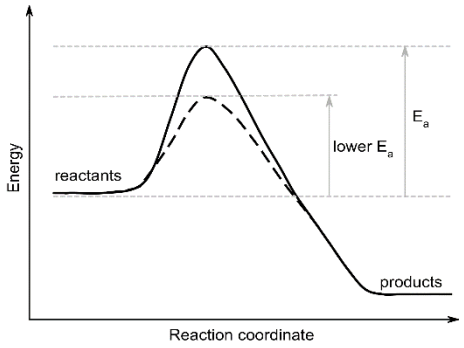

Figure 4 E_a of a chemical reaction

2.2.1.3 Heat management

Thermodynamically, the chemical reaction of H_2 and O_2 depicts an exotherm reaction, thus lots of heat is produced. To keep the cell temperature at a suitable value and to maintain the efficiency of the FC this heat has to be rejected. The higher the temperature difference between the environment and the FC system, the easier it is to cool the system. This denotes, that operating a HT-PEM FC requires a smaller cooling system than for low temperature operation [18]. The simplification of the cooling system and further using the heat for other purposes, such as warm water generation or a steam gas reformer, can significantly increase the efficiency of a FC system [18].

2.2.1.4 Water management

In addition to the heat management, also the water management in HT-PEM FCs is simplified. As already brought up, to provide high proton conductivity of the PFSA membrane in LT-PEM FCs, a high water content is necessary. Thus, usually complicated humidifier systems are employed to humidify the fuel and the oxidant. However, too much water inside a FC can cause flooding, which means blocking of the porous structures of CL and GDL or the gas transport channels in the bipolar plates. The modification of the membrane employed in HT-PEM FCs makes an operation up to 200 °C feasible without any humidification [18]. Since no humidification of the gases and the membrane is necessary the design of PEM FC can be simplified.

2.2.1.5 Polymer electrolytes for HT-PEM FCs

Due to the high temperature operation, alternative polymer electrolyte membranes are necessary. Consequently, PA doped PBI (polybenzimidazole) membranes receive most attention as they offer high mechanical strength, thermal and chemical stability and high proton conductivity at elevated temperatures in HT-PEM FCs [20]. In terms of structure, PBI is an amorphous thermoplastic polymer with a glass transition temperature above 400 °C [21]. Therefore, this material is successfully implemented in HT-PEM FCs. Doping PBI with H_3PO_4 results in a salt by protonation of the imine nitrogen at the imidazole ring. Per monomeric unit of the polymer two H_3PO_4 molecules adsorb, while free PA is needed to provide a high proton conductivity [18]. The structures of PBI and PA doped PBI are visualized in Figure 5.

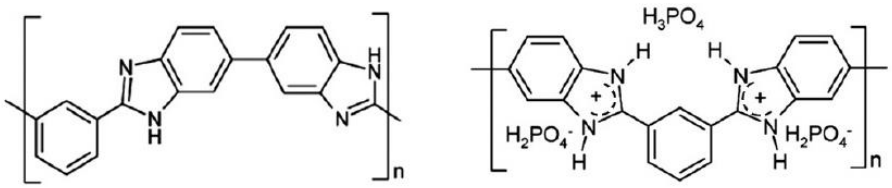

Figure 5 Chemical structure of PBI (left) and PA doped PBI (right) membranes [21]

Although a H_3PO_4 doped PBI membrane is the commonly used electrolyte in HT-PEM FCs there is still one important drawback, which has to be addressed. PA is not stable during operation and undergoes reduction to phosphate species which tend to adsorb on the catalyst surface. As a result, its active sites for the reaction are occluded and the catalytic activity degrades [8]. This major issue will be discussed in detail in the following section 2.2.2.2.

2.2.2 Drawbacks of HT-PEM FCs

2.2.2.1 Catalyst degradation

As of now, the state-of-the-art anode and cathode catalysts for PEM FCs are based on Pt supported on a carbon matrix (Pt/C) to ensure a high electrochemical surface area (ECSA). Commercialization of PEM FCs is still significantly restricted by high Pt loadings on the cathode to counteract performance losses, hence making the whole FC system quite expensive. While the Pt loading at the anode amounts to 0.1 mg cm^{-2} or less, the cathode loading is usually

several times higher. In HT-PEM FC technology even higher loadings are used [22]. Principally, some problems of carbon supported Pt catalysts still need to be addressed:

- Carbon corrosion [23]
- Pt particle agglomeration through Ostwald ripening [24]
- Pt dissolution and detachment [24]

Therefore, the catalyst undergoes severe degradation during operation, which tends to cause a decrease of the ECSA, thus declining the electrocatalytic performance. Especially during long-term operation at high temperatures, the Pt nanoparticles (NPs) tend to agglomerate after the coalescence mechanism, in which small metal particles move together forming larger particles (see Figure 6) [11].

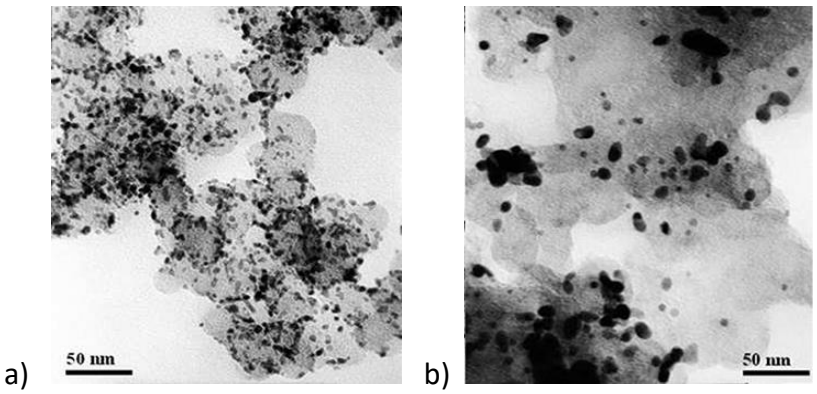

Figure 6 TEM images of cathode catalyst layer a) before and b) after long-term operation (1500 CV cycles) [9]

2.2.2.2 Influence of phosphoric acid on oxygen reduction reaction activity

The employment of PA impregnated membranes in HT-PEM FCs is one of the major drawbacks concerning the electrocatalytic performance of the Pt catalyst. As already mentioned the PA is not stable during HT-PEM FC operation and undergoes reduction to phosphorous compounds in a lower oxidation state. These impurities partially cover the Pt catalyst surface and inhibit its active sites for catalytic activities [26].

The formation of such phosphates is attributed to the electrochemical reduction of H_3PO_4 as well as to its reduction by H_2 where Pt acts as catalyst of this process [26]. It is assumed, that the formation takes place at potentials corresponding to H_2 evolution and at potentials in the double layer region between 0.4 and 0.7 V (see Figure 12) [26]. In aqueous solution the

reduction products are deprotonated dihydrogen phosphate ($H_2PO_4^-$) ions, hydrogen phosphate (HPO_3^{2-}) ions as well as phosphate ions (PO_4^{3-}). Among them, the $H_2PO_4^-$ ion is assumed to be the strongest adsorbate on the Pt surface [27]. The adsorption mechanism itself follows the principle of chemisorption. Chemisorption involves the formation of strong bonds between the molecules being adsorbed and specific surface regions, which are known as active sites. Depending on the concentration of adsorbate molecules a continuous monolayer is formed irreversibly throughout the catalyst surface. One way to deal with cathode catalyst poisoning by H_3PO_4 is to embed the catalyst in a thin film of a conducting polymer that can offer improved tolerance toward surface-active phosphate ions [28]. This possibility is further named and discussed in section 2.3.2.

2.3 Catalysis in HT-PEM FCs

During the last two decades major efforts have been dedicated to find new catalysts, which provide promising catalytic activity and stability within the corrosive operation conditions of HT-PEM FC based systems. Approaches to reach these requirements depict the alloying of the Pt NPs with late transition metals, the modification with other species, the optimization of the catalyst geometric structure or the development of new supporting materials [29]. Another strategy that addresses both the activity and durability issue is the pre-adsorption of organic functional groups forming an organic metal complex through direct polymerization [30].

2.3.1 Platinum alloys for oxygen reduction reaction

In search for enhanced ORR activity an appropriate catalyst would bind O_2 molecules neither too strong nor too weak [31]. Alloys of Pt with late transition metals (e. g. Co, Cr, Ni etc.) are generally more active towards ORR [17]. The improved activity is attributed to two effects, which lead to changes in the electronic structures of the Pt overlayers. The transition metals induce a *ligand* or *strain effect* [32]. Ligand effects originate from bonding interactions between the active Pt atoms and the alloying metal atoms. This weakens the binding of O_2 intermediates of the ORR on the catalyst surface. Strain effects derive from a compressed arrangement of the Pt overlayers because of disorders imposed by shorter interatomic distances of the alloying metal atoms that are located beneath [32]. This lateral changes bring

about a shift of the d-band center, resulting in a surface that adsorbs O_2 species less strongly than unstrained Pt [33]. For example, Pt alloys such as Pt-Co exhibit a downshift of the d-band center compared with that of Pt. As a result, hydroxide ions but also phosphates, which stem from the PA doped PBI membrane employed in HT-PEM FCs, are less strongly adsorbed [8].
In contrast, Pt-Au alloys for example, show a totally different behavior. In their structure the d-band center of the Pt is upshifted, but however, these Pt-Au alloys still show improved ORR activity in acid electrolyte compared with pure Pt [8]. This could be explained by a geometric effect: hydroxide and phosphate species preferentially adsorb on three-fold Pt sites whose presence is lower in Pt-Au alloys because the Pt atoms are isolated by the Au atoms [8] .
Typically, these Pt alloys are several times more active than pure Pt. The performance of such NPs is effective when their size lies in the range of 2-5 nm and will be dramatically enhanced when their size is around 1 nm [34]. Although it is known that these Pt-transition metal catalysts are still prone to corrosion under PEM FC operating conditions, their application in FCs is of high interest, as they contribute to the enhancement of catalytic activity [33].

2.3.2 Polyaniline decorated platinum catalysts for oxygen reduction reaction

Conductive polymers with polyaromatic backbone, including PANI, received great attention in the last two decades due to their unique properties [35]. These organic compounds are composed of monomers, which have extended π-conjugated structures that ensure electron conductivity under certain conditions (doping). PANI consists of aniline monomer units, which are built up of reduced (y) and oxidized (1-y) blocks (see Figure 7) [36].

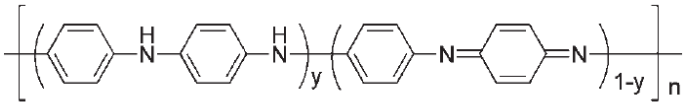

Figure 7 Molecular structure of PANI, reprinted from [36]

Depending on the oxidation state PANI shows different properties like reversible insulator-to-metal transition and electrochromic behavior [37]. In addition to its high electrical conductivity it is a good proton conductor in acidic media. High corrosion resistance and

workability, environmental stability and low costs represent other favorable properties. PANI could be synthesized via electrochemical or chemical polymerization, whereas latter represents a straight-forward procedure. The chemical synthesis of PANI is an oxidative polymerization of aniline monomers, whereby ammonium persulfate (APS) is most commonly used as oxidant. Usually, this polymerization is conducted in acidic media, which leads to PANI in the form of emeraldine (one possible oxidation state) [36]. The combination of excellent features and the straight-forward manufacturing makes PANI useful for various applications including microelectronic devices and sensors, batteries, supercapacitors, FCs and many others [36].

Due to its unique π-conjugated structure, PANI represents a favorable functionalization molecule for Pt based catalysts. Pt NPs dispersed in conducting PANI films have been recognized as valuable catalysts for FCs with high activity and stability [38]. Proceeding via an oxidative coupling polymerization of its monomers, aniline forms a thin layer on the carbon surface of a Pt/C catalyst, which acts as some kind of a protector against degradation treats. A simplified version of the reaction mechanism for synthesizing a PANI-decorated Pt/C catalyst (Pt/C@PANI) is illustrated in Figure 8.

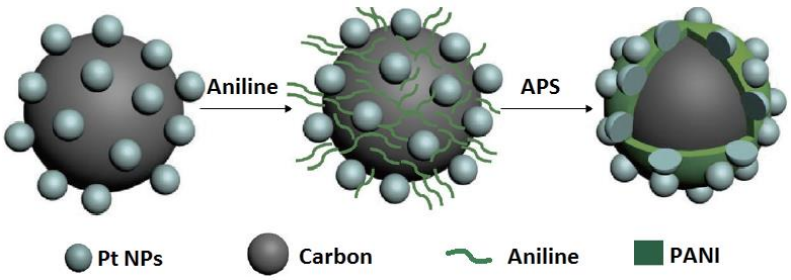

Figure 8 Schematic reaction procedure of a Pt/C@PANI catalyst, reprinted from [9]

In the course of the polymerization, the aniline monomers are adsorbed on the carbon surface via π-π conjugation between aniline and the carbon support and are then polymerized at the carbon surface in the presence of APS in acidic media. In this modified catalyst system, the PANI shell layer selectively covers the surface of the carbon rather than that of Pt, hence not limiting the catalyst's activity [9].

Keeping in mind that the activity of Pt based cathode catalysts in HT-PEM FCs is significantly impaired in the presence of H_3PO_4 due to adsorption of phosphate species on the catalyst surface, this polymer film plays three important roles [39].

First, as the carbon support is totally embedded in the PANI film, the polymer impedes the direct contact between the carbon support and the corrosive environment of the electrolyte. Thus, PANI inhibits carbon oxidation [39]. Secondly, the PANI film strengthens the interaction between the Pt NPs and the carbon support, i.e. it provides a spatial separation of the Pt particles, hence Pt particle agglomeration is inhibited [39]. Last, the electron delocalization between the PANI and the Pt NPs changes the electronic configuration of the Pt NPs. PANI interacts with Pt NPs and carbon either via three carbon atoms or via one nitrogen and two carbon atoms at the same benzene ring. In a Pt/C@PANI catalyst the binding energy of the $4f_{7/2}$ orbital of Pt is shifted to a higher binding energy relative to the $4f_{7/2}$ energy level of the Pt/C catalyst. This shift refers to the electron delocalization between the d-orbitals of the Pt NPs and the π-conjugated aromatic system of PANI [9]. The resulting lowered d-band center and the mentioned raised energy level favor the electron transfer between the Pt/C@PANI catalyst and oxygen because of a reduced gap between the O_2 LUMO (lowest unoccupied molecular orbital) and the Pt/C@PANI catalyst HOMO (highest occupied molecular orbital). Therefore, the desorption of O_2 intermediate species on the catalyst surface is facilitated [39].

In addition, as the electron delocalization makes it more difficult for the Pt NPs to lose or to release electrons, this aggravated oxidation leads to weaker bonds between the adsorbing phosphate species and the Pt surface [28]. In both cases, i.e. simplified desorption of O_2 species and phosphates, the active sites for the ORR are provided and the catalytic activity increases.

Chen and co-workers report that the activity and durability of PANI decorated Pt/C catalysts depends on the thickness of the PANI film [9]. The film thickness is directly related to the content of PANI. Excessive PANI contents incorporate the Pt NPs into the polymer network. Consequently, less or even no ECSA is present in the catalyst system. On the contrary, too low PANI contents do not show any improved catalytic activities [9]. Greatest enhancement of electrocatalytic activities was observed at a shell layer thickness between 2.5 nm to 5.0 nm (see Figure 9). This corresponds to a PANI content in weight percent (wt%) of 20 and 30%, respectively [9].

Figure 10 depicts the significantly enhanced durability of a Pt/C@PANI catalyst compared to that of the state-of-the-art Pt/C catalysts, after determining a suitable content of PANI. After 1500 potential sweep cycles, the ESCA of the Pt/C catalyst decreased three times more than the ECSA of the Pt/C@PANI catalyst.

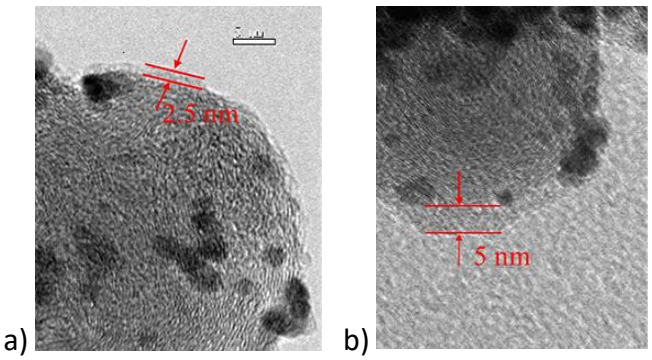

Figure 9 HR-TEM images of catalysts with different PANI contents [9]

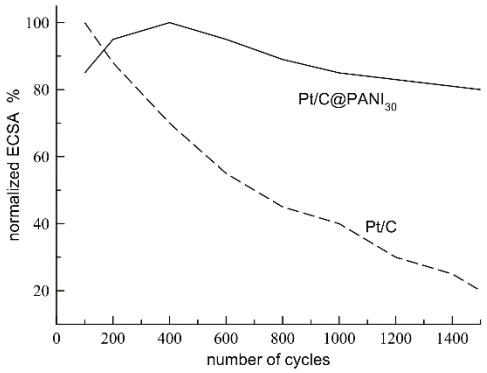

Figure 10 ECSA of Pt/C and Pt/C@PANI after 1500 potential sweep cycles between 0.0 and 1.2 V vs. RHE at a scan rate of 50 mV s^{-1} [9]

By comparing the morphologies of Pt/C and Pt/C@PANI in Figure 11, less particle agglomeration is observed in the case of the PANI functionalized catalyst, confirming that PANI decorated catalyst systems are more stable than conventional Pt/C.

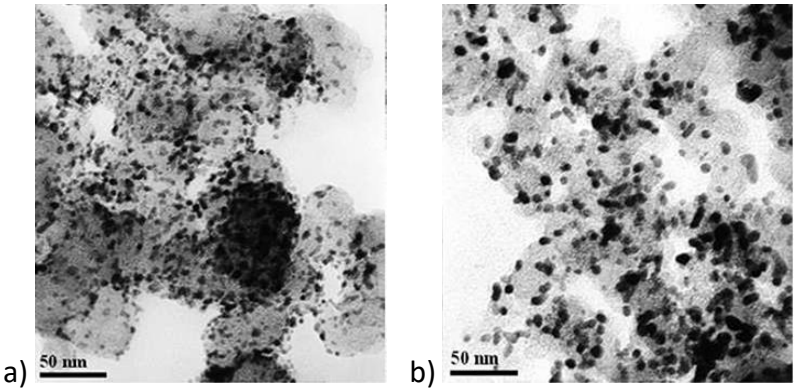

Figure 11 a) TEM images of uncycled Pt/C@PANI catalyst and b) the Pt/C@PANI catalyst after 1500 cycles [9]

2.4 Electrochemical ex-situ characterization technique

A significant advancement in catalyst research for the development of PEM FC MEAs was achieved by the development of the rotating disk electrode (RDE) method [40]. Catalyst testing by means of RDE technology offers a straight-forward alternative to time-consuming and laborious measurements in form of MEAs. It is well suited for the evaluation of a catalyst's stability by potential cycling but also for the study of reaction kinetics [40]. However, to ensure reproducibility the experimental parameters have to be carefully taken into account in order to avoid measurement artefacts and misinterpretation of data [40].

2.4.1 Thin film rotating disk electrode method

Regularly, a three-electrode set-up consisting of a working electrode (WE), a counter electrode (CE) and a reference electrode (reversible hydrogen electrode, RHE) is used. A known amount of catalyst is deposited onto the glassy carbon WE (RDE) and dried via rotation to obtain a homogenous thin film. The film quality is crucial for acquiring reproducible data and performances during cyclic voltammetry (CV) and ORR measurements. For a 10-15wt% Pt catalyst the loading should be between 7 and 30 µg cm^{-2} to ensure good mass transport properties. As electrolyte 0.1 M perchloric acid ($HClO_4$) is used preferably as it generates only non-adsorbing species (ClO_4^-) [41].

At the beginning of a measurement the surface of the tested catalyst has to be cleaned by several potential cycles to obtain a steady current-potential diagram. Considering Pt alloys, it is important to note that the non-noble metal is mostly leached out of the surface if no prior

leaching was performed during catalyst synthesis. The overall quality of the measurement is significantly influenced by the thin film quality on the RDE, the purity of the electrolyte and gases and the cleanliness of the glass ware and the electrodes [41].

Figure 12 illustrates a typical cyclic voltammogram (CV) recorded in nitrogen (N_2) saturated electrolyte with non-rotating WE to determine the ECSA of the catalyst. As in N_2 saturated electrolyte no electroactive species are present only Pt-H oxidation and reduction and Pt-O and Pt-OH formation and reduction can be observed. The first peak of the Pt-H oxidation from 0.1 to 0.2 V is assigned to the Pt(110) surface and the broader peak at 0.3 V to the Pt(111) surface [8]. At potentials above 1.2 V O_2 evolution and below 0.0 V H_2 evolution occurs.

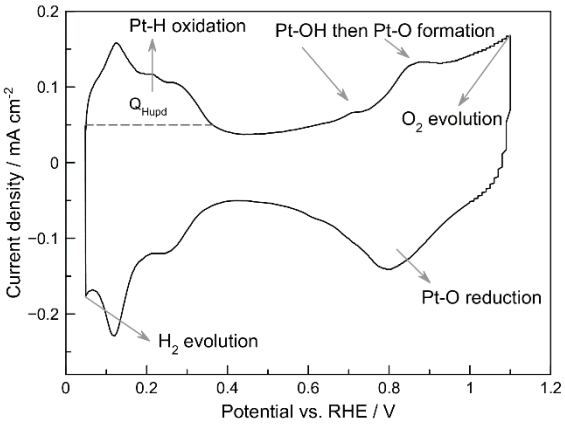

Figure 12 CV recorded in N_2 saturated electrolyte to determine the charge of the H_{upd} area [41]

For the calculation of the ESCA, the charge Q_{Hupd} of the H_2 desorption area was determined (H_{upd}) by integrating the area under the Pt-H oxidation peak (see Figure 12). According to Eq. 9 a conversion factor Q_{Pt} of 210 µC cm_{Pt}^{-2} is considered. To obtain the ECSA in cm^2 mg_{Pt}^{-1} the A_{active} is divided through the product of Pt loading l_{Pt} applied on the RDE and the area of the RDE A_{RDE}.

$$A_{active} = \frac{\mathrm{Q_{Hupd}}}{\mathrm{Q_{Pt}}} \qquad \text{Eq. 9}$$

$$ECSA = \frac{A_{active}}{\mathrm{l_{Pt}} * A_{RDE}} \qquad \text{Eq. 10}$$

Q_{Pt} is the electrical charge generally associated with the adsorption of a monolayer of H_2 on a pure Pt surface [41]. ECSA measurements could be taken at different instances, before and after the presence of contaminants in the electrolyte, and the resulting ECSAs at those instances are compared.

The electrocatalytic activity of catalysts is best compared by their mass activity (MA) and area specific activities, also named as specific current density (SCD) [41]. For their investigation, polarization curves of the ORR in O_2 saturated electrolyte with rotating RDE are recorded. To make sure that only currents related to the ORR and not to Pt-O, Pt-H, Pt-OH formation and decomposition are obtained, the CV cycle measured in N_2 saturated electrolyte is subtracted from the ORR polarization curve. Further, the potential is corrected by the reference hydrogen potential (V_{RHE}) and by the internal resistance of the electrolyte ($\Omega_{electrolyte}$). Figure 13 depicts the importance of the correction procedure.

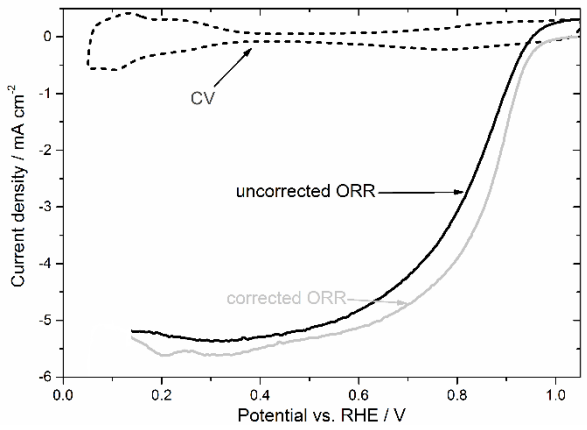

Figure 13 Influence of the applied correction on the ORR, reprinted from [11]

For the definition of the MA and the SCD the mixed kinetic diffusion controlled region between 0.7 and 1.0 V_{RHE} and the diffusion limited current density region between 0.2 and 0.4 V_{RHE} are of relevance. Usually, the potential at 0.9 V_{RHE} is used to calculate MA and SCD as it lies within 10 to 80% of the diffusion limited current depending on the rotation speed of the RDE [40]. After correction, MA and SCD are calculated as follows.

$$\mathrm{SCD} = \frac{\mathrm{i_k}}{A_{active}} = \frac{\mathrm{i_d} * \mathrm{i_{0.9}}}{\mathrm{i_d} - \mathrm{i_{0.9}}} * \frac{1}{A_{active}} \quad \text{Eq. 11}$$

$$\mathrm{MA} = \mathrm{i_k} * \frac{1}{\mathrm{l_{Pt}}} \quad \text{Eq. 12}$$

Together witch the diffusion limited current i_d and the current at 0.9 V_{RHE} ($i_{0.9}$) the kinetic limited current i_k is calculated. The SCD of a catalyst is determined via normalization of the current i_k with A_{active}. The MA of a catalyst in A mg^{-1} results from division of the i_k through l_{Pt}.

For an electrochemical reaction, where the current is limited by diffusion, i_d can be related to the rotation rate of the RDE applying the Levich equation (Eq. 13) [34]. When the solution contains only the reduced molecule species the equation can be written as

$$\mathrm{i_d} = -0.62 * \mathrm{n} * \mathrm{F} * \mathrm{A} * \mathrm{D_R^{\frac{2}{3}}} * \omega^{\frac{1}{2}} * \mathrm{v^{-\frac{1}{6}}} * \mathrm{C_R} \quad \text{Eq. 13}$$

where n is the number of electrons transferred during the ORR, F is the Faraday constant (96485 C mol^{-1}), A is the electrode area (m^2), D_R is the diffusion coefficient (m^2 s^{-1}), ω is the rotation speed (rad s^{-1}), v is the kinematic viscosity of the electrolyte (m^2 s^{-1}) and C_R is the bulk concentration of O_2. According to this equation the number of electrons transferred during reduction (or oxidation) could be determined. Plotting the values of i_d against the square root of ω the graph should represent a linear relationship.

3 Experimental

3.1 Materials and methods

3.1.1 Chemicals

All chemicals were used as purchased without further purification.

- H_2PtCl_6 * $6H_2O$, metal basis 99.95%, Pt 39.72%, by Alfa Aesar Premion®
- $Co(NO_3)_2$ * $6H_2O$, metal basis 99.999%, by Sigma Aldrich
- KBr, p.a., ACS, by MERCK KGaA
- $NaBH_4$, by Alfa Aesar
- Aniline, ACS ≥ 99.5%, by Sigma Aldrich
- Ammonium persulfate, APS, by Merck
- CABOT Vulcan XC72R (Carbon Black), GP-3820, CAS No. 1333-86-4, by Cabot Corporation
- Ultrapure H_2O 18 MΩ, Barnstead Nanopure Water Purification System
- 2-Propanol ASC ≥ 99.8%, by Sigma Aldrich
- $HClO_4$ acid concentrate 0.1 mol for 1 l standard solution, by Sigma Aldrich (Fixanal, Fluka® Analytical)
- ortho-H_3PO_4 ROTIPURAN® ACS >85%, by Carl Roth ®
- H_2SO_4, 96% Ultrapur., by Merck
- Pt/C, platinum nominally 50% on carbon black, by Alfa Aesar
- Pt_3Co/C, 30wt% Pt-Co loading, by Sigma Aldrich
- Alumina suspension, 0.05 µm, by MasterPrep Bühler
- Nitrogen, 5.0, by Air Liquide
- Oxygen, 4.5, by Air Liquide
- Hydrogen, 5.0, by Air Liquide

3.1.2 Instruments and equipment

- Potentiostat/Galvanostat/ZRA Reference 600, by GAMRY Instruments
- Rotating electrode RDE710, 100-240 VAC, 50/60 Hz, 2 A, by GAMRY Instruments
- RDE: ring disk electrode (glassy carbon area 0.196 cm^2), Model AFE5T050GC, Serial No. 20/34, by Pine Research Instrumentation
- RDE: ring disk electrode (glassy carbon area 0.196 cm^2), Model AFE5T050GC, Serial No. 20/35, by Pine Research Instrumentation
- RHE: reversible hydrogen electrode (gaskatel HydroFlex), by Gaskatel Gesellschaft für Gassysteme durch Katalyse und Elektrochemie mbH
- Counter electrode: platinized titanium rod, by Bank Elektronik – Intelligent controls GmbH
- Julabo, model MC, class: III, AC: 190-253 V/50-60 Hz, DIN: 12876, by Julabo Labortechniken GmbH
- Ultrasonic bath Bandelin Sonorex, by BANDELIN electronic GmbH & Co. KG
- Ultrasonic processor UP400S, by hielscher Ultrasound Technology
- Scale: Sartorius BP 110S max. 110 g, by Sartorius AG
- Magnetic stirrer: Heidolph MR Hei-Tech, by Heidolph Instruments GmbH & Co. KG
- Drying oven: DRY-line, by VWR
- Centrifuge: Labofuge 400, by Heraeus
- Lab furnace: Jumo Dicon 501, Elsklo
- Pipette, 1000 µl, pipet4u ® Performance, by AHN Biotechnology GmbH
- Pipette, 2-20 µl, by Phoenix Instruments
- Pipette tip: 1000 µl, PE, by Eppendorf AG
- Pipette tip: 250 µl, PE, by Eppendorf AG

3.1.3 Software

- Gamry Framework Version 6.25, by Gamry Instruments
- Gamry Echem Analyst, by Gamry Instruments
- My Gamry Data, by Gamry Instruments
- Microsoft Office Excel 2010, by Microsoft
- MagicPlot Pro

3.2 Catalyst preparation

A commercial Pt_{50}/C and an in-house Pt_{20}/C catalyst as well as a commercial $Pt_{22.5}Co$/C and an in-house $Pt_{15}Co$/C catalysts were functionalized with PANI forming a thin polymeric film around the NPs. Following the supporting information of *S. Chen* and coworkers [42], samples with different PANI contents were prepared. The percentage of PANI was adjusted to the wt% of Pt in the sample, which is denoted by the indices at Pt, and is summarized in Table 1.

Table 1 Wt% of total metal content, of Pt and of PANI in Pt/C@PANI and Pt-Co/C@PANI catalysts

Sample	Wt% total metal content	Wt% Pt	Wt% PANI
Pt_{50}/C@PANI	50	50	10, 20, 30
Pt_{20}/C@PANI	20	20	30
$Pt_{22.5}Co$/C@PANI	30	22.5	20
$Pt_{15}Co$/C@PANI	20	15	20

3.2.1 PANI synthesis

All PANI samples were prepared identically as given in the following example of Pt_{50}/C with 20wt% PANI (Pt_{50}/C@$PANI_{20}$). The synthesis was performed in an ice bath. 20 mg of aniline monomer were dissolved in 20 ml 0.5 M H_2SO_4 aqueous solution by ultrasonic blending. 80 mg of Pt_{50}/C catalyst were dispersed in it and the mixture was stirred ultrasonically 2 hours to achieve a homogenous dispersion. Ammonium persulfate (APS) (n_{APS}:$n_{aniline}$ = 1:1) was

dissolved in 0.5 M H_2SO_4 and added dropwise under stirring to the dispersion. The polymerization was conducted in a refrigerator overnight. The obtained product was centrifuged 3 times at 3500 rpm and washed with an ethanol/water solution (1:1) after each run. Finally, the obtained black precipitate was dried at 40 °C.

3.2.2 Platinum catalyst synthesis

In-house Pt_{20}/C and $Pt_{15}Co$/C catalysts were synthesized following a surfactant-free method, the so called Bromide Anion Exchange (BAE) method [43]. The total amount of metals was set to 20wt% for both. The ratios of metals, which showed the best results are given in Table 2. It is expected that an excess of cobalt is removed during post-preparation treatment leading to Pt_3Co/C.

Table 2 Ratios of metals for in-house catalyst preparation

Sample	Ratio Pt : Metal
Pt_{20}/C	1:0
$Pt_{15}Co$/C	1:5

The metal precursors were dissolved in ultrapure H_2O using a magnetic stirrer. Then, KBr (n_{KBr}/n_{Metals} = 1.5) was added to the solution. After complete dissolution, the supporting material Vulcan XC72R was added by using an ultrasonic processor for 45 minutes providing a homogenous dispersion. Afterwards, a freshly prepared $NaBH_4$ solution (reducing agent) (n_{NaBH4}/n_{Metals} = 15) was added dropwise. The reaction continued for 2 hours at 40 °C under ultrasonic homogenization.

Post treatment

After the reduction process the samples were treated in different ways, as follows:

- No treatment: The reaction mixtures of Pt_{20}/C samples were centrifuged for 30 minutes at 3500 rpm 3 times, whereby the precipitate was washed in ultrapure H_2O after each run. Finally, the precipitate was dried at 40 °C.

- Acid leaching and heat treatment: The $Pt_{15}Co/C$ samples were leached in 10vol% H_2SO_4 for 30 min. Afterwards, the samples were washed in ultrapure H_2O and centrifuged for 30 minutes at 3500 rpm 3 times. Finally, the precipitate was dried at 40 °C. After the drying, the alloys were heat treated in a lab furnace for 45 min at 240 °C, heated with a ramp of 5 °C min^{-1}.

3.3 Electrochemical ex-situ studies

CV and ORR measurements were executed at 30 °C. Before performing any electrochemical measurement, all glassware was cleaned in boiling ultrapure H_2O. The glassy carbon RDE was polished using a 0.05 µm alumina suspension and washed clean with ultrapure H_2O.

The experiments were carried out using a potentiostat and a rotating disk electrode assembly, which is a combination of a rotator and an electrode obtained from Gamry Instruments. Figure 14 represents the applied standard 3-electrode electrochemical set-up.

a)  b) 

Figure 14 a) Standard 3-electrode set-up for ex-situ electrochemical measurements, b) deposited catalyst dispersion on RDE

Thereby the working electrode was a commercial glassy carbon disk electrode of 5 mm diameter (area 0.196 cm^2), as CE a platinized titanium rod was used. The reference electrode was a calibrated RHE and all reported potentials are in reference to the RHE. In order to enable measurements at different conditions this set-up was completed with gas inlets for N_2, O_2 and H_2, which was positioned in a way to ensure that any bubbles could not interfere with the

catalyst surface on the RDE while introducing gas into the electrolyte. As electrolyte 0.1 M $HClO_4$ aqueous solution prepared with ultrapure H_2O was used.

In order to prepare a catalyst ink, a defined amount of catalyst was dispersed in 3 ml of a water/isopropanol mixture (3:7) using an ultrasonic bath until a homogenous dispersion was obtained. The glassy carbon disk of the RDE (area of 0.196 cm^2) was then coated with the catalyst dispersion to obtain a total Pt loading of 28 µg cm^{-2} (geometric surface area) Therefore, 10 µl of the prepared catalyst dispersion were pipetted on it (2 x 5 µl) without wetting the surrounding part. The droplet was dried by means of a rotating electrode (700-750 rpm) with the purpose to obtain a very thin catalyst film.

The CV measurements were conducted in N_2 saturated electrolyte. After immersing the working electrode into the electrolyte solution, the internal resistance drop of the electrolyte was measured. The catalysts were pretreated using 80 cyclic voltammetry scans (cleaning cycles) in order to remove undesired contaminations from the catalyst surface. Normally, this number of cycles was enough to obtain a stable CV. Therefore, the potential was swept between 0.05 and 1.10 V_{RHE} at a scan rate of 50 mV s^{-1}. Afterwards, three analysis cycles were recorded in the same potential range at a scan rate of 10 mV s^{-1}.

ORR activity measurements were performed in an electrolyte saturated with O_2. Three cycles between 0.05 and 1.10 V_{RHE} at a scan rate of 10 mV s^{-1} were performed at different rotation rates (400-2000 rpm). The potential of the RHE was controlled by performing the H_2 evolution reaction on Pt in $HClO_4$ electrolyte saturated with H_2. A summary of the performed electrochemical ex-situ measurements is given in Table 3.

Accordingly, CV and ORR measurements were done in 0.1 M $HClO_4$ electrolyte containing 0 mM H_3PO_4, then 1 mM H_3PO_4 and 5 mM H_3PO_4 to investigate tolerance toward PA.

Table 3 Summary of the performed electrochemical ex-situ measurements

	Lower vertex vs. RHE / V	Upper vertex vs. RHE / V	Scan speed / mV s^{-1}	Rotation / rpm	No. of cyles
Cleaning	0.05	1.10	50	0	80
CV	0.05	1.10	10	0	3
ORR	0.05	1.10	10	400, 600, 900, 1200, 1600, 2000	3

3.3.1 Data treatment

The software Echem Analyst from Gamry was used to determine the charge of the H_{upd} peak of the second analysis cycle. To obtain Q_{Hupd} in coulomb (C) the integrated area was divided by the scan rate in V s^{-1}. All CV analyses were corrected for reference potential (V_{RHE}) and the currents were normalized relative to the geometric surface area of the RDE (0.196 cm^2) giving the results of the ECSA in cm^2 mg_{Pt}^{-1} (see Eq. 10).

The second cycle of ORR experiments at each rotation speed was used to determine the SCD in mA cm^{-2} and the MA in A mg_{Pt}^{-1}. After correction for the V_{RHE} and $\Omega_{electrolyte}$, only the positive anodic sweep of the ORR was plotted against the current density and used to determine the SCD and the MA as described in the theory (see section 2.4.1).

The number of electrons transferred during the ORR was calculated by means of the Levich equation (Eq. 13) with the following parameters:

A active area of electrode [0.196 cm^2]

D_R diffusion coefficient [$1.9*10^{-5}$ cm^2 s^{-1}]

ω rotation of electrode [rad s^{-1}]

v kinematic viscosity [$8.93*10^{-3}$ cm^2 s^{-1}]

C_R bulk concentration of O_2 [$1.18*10^{-6}$ mol cm^{-3}]

4 Results and discussion

With the aim to mitigate problems referring to the presence of PA in HT-PEM FCs, Pt based catalysts decorated with PANI were prepared.

Chen and co-workers [42] obtained best results with Pt catalysts containing 30wt% of PANI. Accordingly, the first experimental step was to evaluate the most suitable content of PANI on a commercial Pt_{50}/C catalyst. After the investigation of a 30wt% PANI-decorated commercial Pt catalyst (Pt_{50}/C@$PANI_{30}$), catalyst samples with 20 and 10wt% PANI were prepared. Since the results of them were promising, also an in-house Pt catalyst containing 20wt% of Pt (Pt_{20}/C) was functionalized with PANI.

As *A. Schenk et a*l. presented Pt-Co alloys (Pt-Co/C) with a high catalytic activity compared to that of pure Pt, it was further investigated if these alloys exhibit even higher catalytic activity when being functionalized with PANI. With respect to the in-house prepared Pt_{20}/C@$PANI_{30}$ sample an in-house $Pt_{15}Co$/C catalyst (20wt% total metal content) was also decorated with PANI ($Pt_{15}Co$/C@$PANI_{20}$). The catalytic activities of all PANI decorated catalysts were compared to the commercial and undecorated equivalents. The indices at Pt denote the content of Pt, the ones at PANI indicate the content of PANI (in wt%). Certainly, the percentage of PANI was adjusted to the amount of Pt.

Electrochemical characterization of the prepared catalysts was performed by CV measurements in N_2 saturated electrolyte and ORR measurements in O_2 saturated electrolyte. All experiments were done in 0.1 M $HClO_4$ electrolyte containing 0 mM, then 1 mM and 5 mM H_3PO_4. For each sample the ORR activity was recorded with a rotating electrode at different rotation rates between 400 and 2000 rpm.

The average results of three CV and ORR measurements for each catalyst sample are discussed in the following sections. In addition, the three most important parameters to quantify the electrocatalytic activity, i.e. ECSA, MA and SCD, are summarized there. To compare the measurements to each other ORR polarization curves were evaluated at a rotation rate of 1600 rpm. The voltage is always given in regard to RHE and corrected for the ohmic resistance of the electrolyte. Furthermore, the number of electrons, which are transferred during the ORR, was determined by using the Levich equation (Eq. 13).

4.1 Pt_{50}/C@PANI catalysts

4.1.1 Influence of PA on the ECSA of Pt_{50}/C and Pt_{50}/C@PANI catalysts

The reduction of the ECSA is attributed to several factors such as Pt agglomeration, and dissolution as well as phosphates adsorption on active sites. In order to identify the most favored PANI content to inhibit PA adsorption, a commercial Pt_{50}/C catalyst was decorated with 30, 20 and 10wt% PANI. Therefore, the synthesis followed an oxidative polymerization of aniline with APS. To investigate the stability of the newly synthesized catalysts, i.e. Pt_{50}/C@$PANI_{30}$, Pt_{50}/C@$PANI_{20}$, Pt_{50}/C@$PANI_{10}$, CV measurements were performed in 0.1 M $HClO_4$ electrolyte containing 0 mM, 1 mM, 5 mM H_3PO_4 and compared to the performance of the undecorated Pt_{50}/C catalyst.

The CV curves of the Pt_{50}/C catalyst are illustrated in Figure 15 and represent the characteristic shape of Pt based catalysts. The graph can be divided into three regions: the adsorption and desorption region of H_2 (0.05-0.40 V vs. RHE), the double-layer region (0.4-0.6 V vs. RHE) and the Pt oxidation region (0.6-1.1 V vs. RHE) [8]. The first difference of the CV curve recorded in $HClO_4$ compared with the CV curves in H_3PO_4 occurs in the region of the H_2 desorption area. In $HClO_4$ the peak between 0.1 and 0.2 V vs. RHE is attributed to the Pt(110), whereas the smooth peak between 0.2 and 0.3 V vs. RHE refers to the Pt(111) [8]. In H_3PO_4 the peak at 0.1 V vs. RHE is weaker, while the peak at 0.2 V vs. RHE is sharper. This results from the adsorption of phosphate ions on the Pt surface [8]. As a result, the overall decrease of the peak in this region leads to a decrease of Q_{Hupd}, thus to a loss of the ECSA. Depending on the concentration of PA the loss of ECSA increases significantly. The calculated values for the ECSA of Pt_{50}/C are given in Figure 15.

The second difference occurs in the region of Pt oxidation and Pt reduction between 0.6 and 1.0 V vs. RHE. Compared to the CV in 0 mM H_3PO_4, the potential of Pt-OH and Pt-O formation in 1 mM and 5 mM PA is shifted to more positive values. This indicates an inhibition of the adsorption of oxygen species and a delayed Pt-O formation by adsorbed phosphate species. That again implies a competitive adsorption of phosphate ions and O_2 species at potentials from 0.4 to 0.8 V vs. RHE [8].

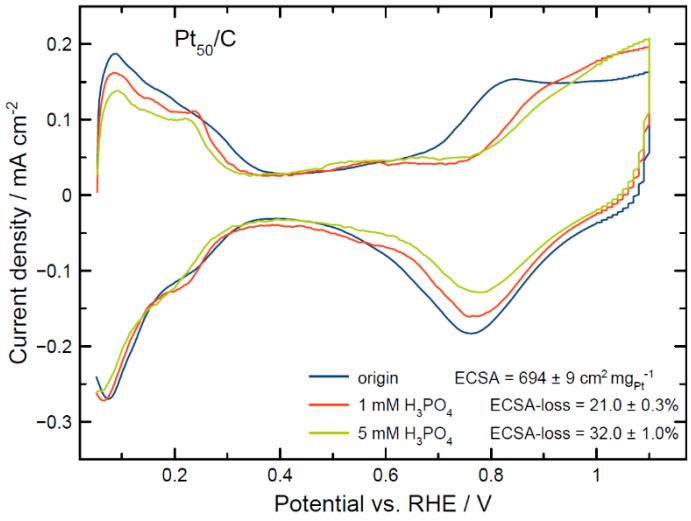

Figure 15 CV curves of Pt_{50}/C catalyst in 0.1 M $HClO_4$ with 0 mM, 1 mM and 5 mM H_3PO_4 (average of 3 measurements)

The CV curves of the PANI decorated Pt_{50}/C samples in 0 mM, 1 mM and 5 mM H_3PO_4 are shown in Figure 16, Figure 17 and Figure 18. Similar to that of the Pt_{50}/C, the area of the H_2 desorption peak declines in the presence of PA in all three CVs. But the ECSA of the Pt_{50}/C@PANI samples lost only 1.00 ± 0.02-15.0 ± 0.3% of its initial area, whereas the Pt_{50}/C catalyst lost 21.0 ± 0.3-32.0 ± 1.0%. Among the PANI decorated Pt_{50}/C catalyst samples, Pt_{50}/C@$PANI_{30}$ exhibits the highest stability in PA containing electrolyte with a decrease of its ECSA by only 1.00 ± 0.02% to 2.00 ± 0.06%. The Pt_{50}/C@$PANI_{20}$ catalyst behaves nearly the same, whereas Pt_{50}/C@$PANI_{10}$ shows the highest loss of ECSA, which is still low compared to that of the pure Pt catalyst. This stability enhancement is confirmed to the unique properties of PANI. As it forms a shell around the catalyst the polymer film protects Pt and carbon and hence prevents carbon corrosion, Pt particle agglomeration and dissolution [9]. Also, due to the electron transfer between Pt and PANI, the catalyst NPs are less oxidized. Thus, O_2 desorption is favored, whereas phosphate species adsorption is inhibited [9]. In addition, the positive influence on the catalysts stability depends on the PANI film thickness, i.e. the PANI content. In the case of Pt_{50}/C@$PANI_{10}$ it is assumed that the PANI content was too low to provide optimal stability against phosphates adsorption [9]. This is indicated by the highest loss of ECSA compared to the other PANI functionalized Pt_{50}/C catalysts.

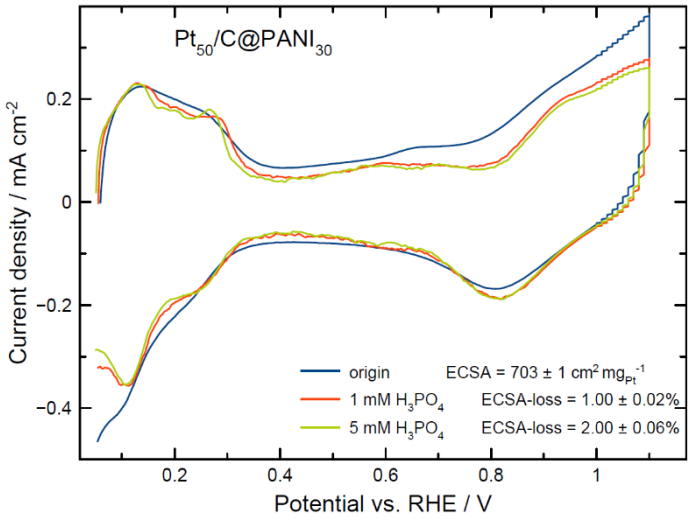

Figure 16 CV curves of $Pt_{50}/C@PANI_{30}$ catalyst in 0.1 M $HClO_4$ with 0 mM, 1 mM and 5 mM H_3PO_4 (average of 3 measurements)

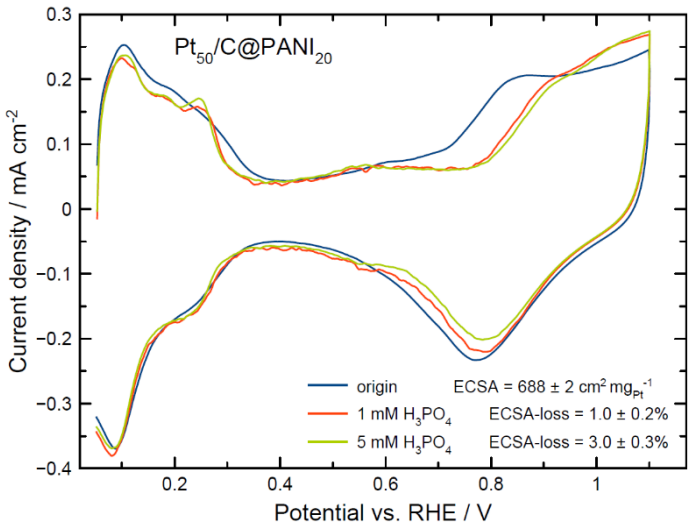

Figure 17 CV curves of $Pt_{50}/C@PANI_{20}$ catalyst in 0.1 M $HClO_4$ with 0 mM, 1 mM and 5 mM H_3PO_4 (average of 3 measurements)

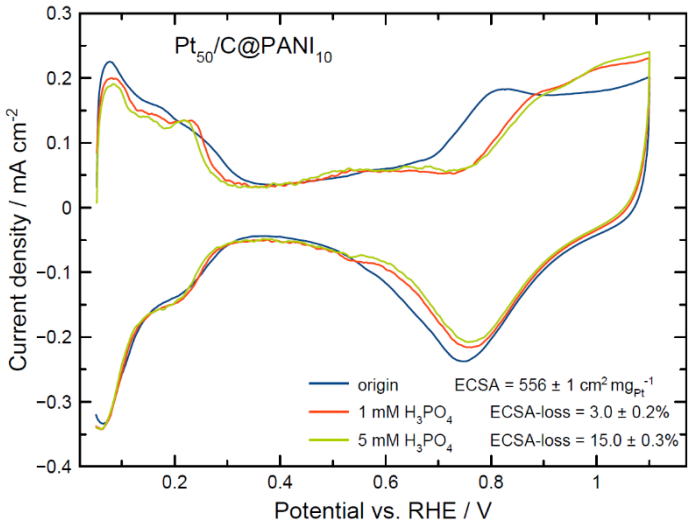

Figure 18 CV curves of $Pt_{50}/C@PANI_{10}$ catalyst in 0.1 M $HClO_4$ with 0 mM, 1 mM and 5 mM H_3PO_4 (average of 3 measurements)

4.1.2 Catalytic activity

Due to the adsorption of phosphate species on the catalyst surface mainly its catalytic activity suffers as these species block active sites for the catalysis of the ORR. ORR polarization curves were recorded in O_2 saturated 0.1 M $HClO_4$ electrolyte with 0 mM, 1 mM and 5 mM H_3PO_4 at different rotation rates (400-2000 rpm). Figure 19 depicts the ORR polarization curves of Pt_{50}/C to spell out the influence of PA on its catalytic activity. The onset potential of the ORR polarization curves recorded in PA exhibit large shifts to lower potentials than the ORR curve in $HClO_4$. This results from the decrease of Pt active sites because of strong adsorption of phosphate ions [8]. The potential shifts have big effect on the i_k at 0.9 V vs. RHE in the kinetic controlled region, as it is marked by the dotted grey line in Figure 19. In this case, the i_k becomes lower. In regard to Eq. 11 and Eq. 12 a negative value of i_k is much favored as higher values for MA result. The current in the diffusion controlled region stays almost constant as it is only affected by different rotation rates.

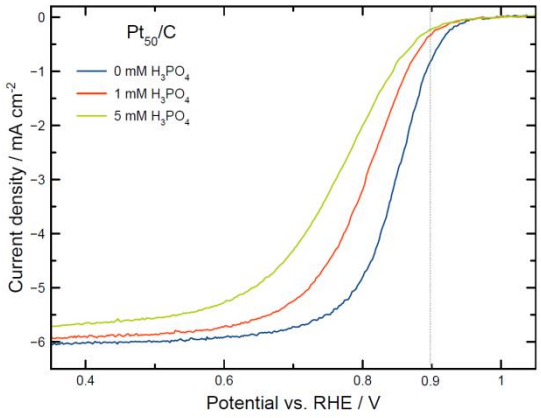

Figure 19 ORR polarization curves of Pt_{50}/C in 0.1 M $HClO_4$ with 0 mM, 1 mM and 5 mM H_3PO_4 at 1600 rpm (average of 3 measurements)

The ORR polarization curves of the PANI decorated Pt_{50}/C catalyst samples are shown below (Figure 20). All of them are compared with the undecorated Pt_{50}/C at each concentration of H_3PO_4. As the CVs already indicate that a PANI content of 20 and 30wt% results in reduced phosphates adsorption, the corresponding Pt_{50}/C@$PANI_{30}$ and Pt_{50}/C@$PANI_{20}$ catalysts confirm increased catalytic activity toward the ORR. By far the best activity toward ORR exhibits the Pt_{50}/C@$PANI_{30}$ catalyst, which was consequently chosen to be the benchmark for further catalyst preparation. The onset potential of Pt_{50}/C@$PANI_{30}$ in 0.1 M $HClO_4$ is significantly shifted to more positive potentials compared to that of Pt_{50}/C (see Figure 20). As there are no phosphate species in the electrolyte the catalytic activity must be improved by the mentioned properties of PANI itself.

In H_3PO_4 the onset potential of Pt_{50}/C@$PANI_{30}$ is less shifted to lower potentials compared to that of Pt_{50}/C (see Figure 20). Hereof, also Pt_{50}/C@$PANI_{20}$ shows favored catalytic activity. This indicates a reduced interaction of H_3PO_4 species with the Pt NPs due to the PANI shell on the catalyst surface [9]. Considering the onset potentials of undecorated Pt_{50}/C in 1 mM and 5 mM H_3PO_4 they are strongly displaced in negative direction because of suffering from PA adsorption. The Pt_{50}/C@$PANI_{10}$ sample shows the lowest catalytic performance among the PANI decorated Pt_{50}/C samples. From the beginning its onset potential represents the lowest potential value. As assumed the PANI content in this catalyst is too low to improve the catalytic activity significantly through the interaction of PANI with the Pt NPs [9]. Nevertheless, the PANI layer around the Pt NPs protects the catalyst as it suffers less than Pt_{50}/C from PA. Hence,

the onset potential of $Pt_{50}/C@PANI_{10}$ in H_3PO_4 containing electrolyte is less strongly shifted in negative direction compared to that of Pt_{50}/C.

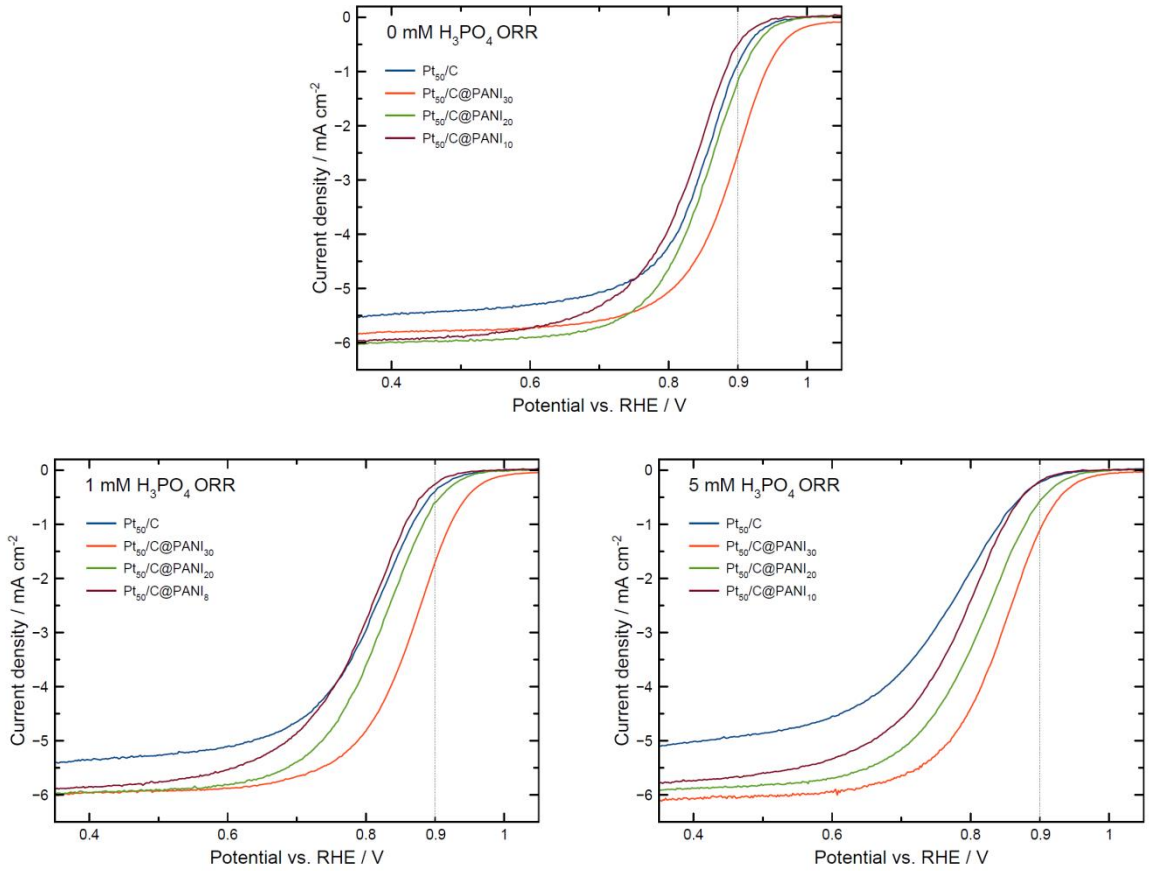

Figure 20 ORR polarization curves of Pt_{50}/C and $Pt_{50}/C@PANI$ samples in 0.1 M $HClO_4$ with 0 mM, 1 mM and 5 mM H_3PO_4 at 1600 rpm (average of 3 measurements)

Further, to determine how the PANI shell affects the ORR kinetics, intrinsic activities, i.e. MA and SCD, for Pt_{50}/C and $Pt_{50}/C@PANI$ samples were calculated according to Eq. 11 and Eq. 12. The MA was obtained from the current density at 0.9 V vs. RHE and the SCD was calculated from the ratio of MA to A_{active} of the corresponding CV cycles.

In Figure 21 the determined values for the MA of Pt_{50}/C and $Pt_{50}/C@PANI$ catalysts of ORR measurements at 1600 rpm and at the overall rotation rates (400-2000 rpm) are illustrated. By decorating the Pt_{50}/C catalyst with an appropriate PANI content the MA was enhanced, also in PA environment. In this case, $Pt_{50}/C@PANI_{30}$ shows the highest MA of 0.063 ± 0.004 A mg^{-1} in pure electrolyte at 1600 rpm, but it exhibits also in 1 mM and 5 mM H_3PO_4 the highest MA of 0.048 ± 0.006 A mg^{-1} and 0.034 ± 0.003 A mg^{-1}. Whereas the MA of

Pt_{50}/C decreases in PA by approximately 50% to 70%, the MA of Pt_{50}/C@$PANI_{30}$ decreases in 1 mM PA by around 24% and in 5 mM by around 46% at 1600 rpm. Also, the Pt_{50}/C@$PANI_{20}$ catalyst exhibits a higher MA than the pure Pt_{50}/C, but a lower one than the Pt_{50}/C@$PANI_{30}$ sample. If the PANI content was too low as in the Pt_{50}/C@$PANI_{10}$ sample no improvement of the MA was achieved, thus it shows the lowest values of MA. This decrease of MA confirms the poisoning effect of Pt based catalysts by phosphates.

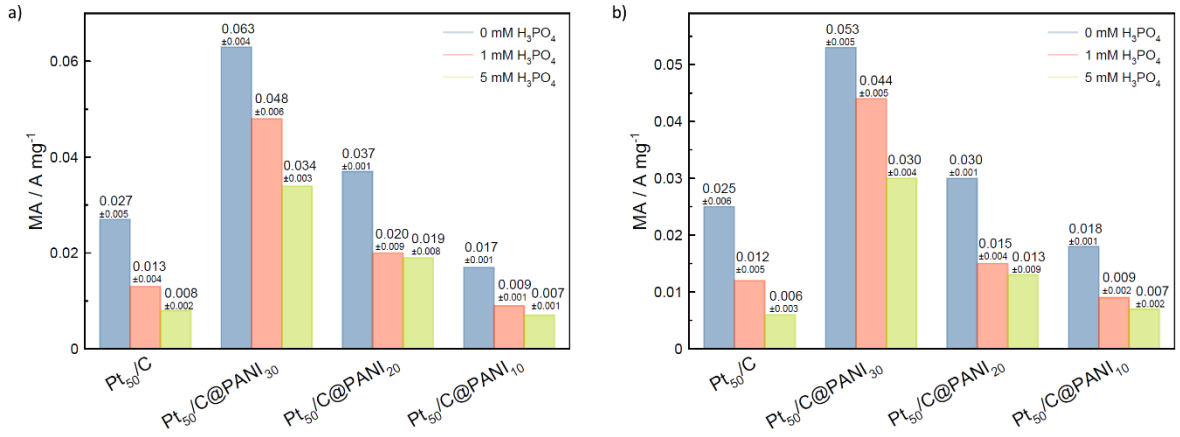

Figure 21 MA of Pt_{50}/C and Pt_{50}/C@PANI catalysts at a) 1600 rpm and b) at the overall rotation rates (400-2000 rpm) (average of 3 measurements)

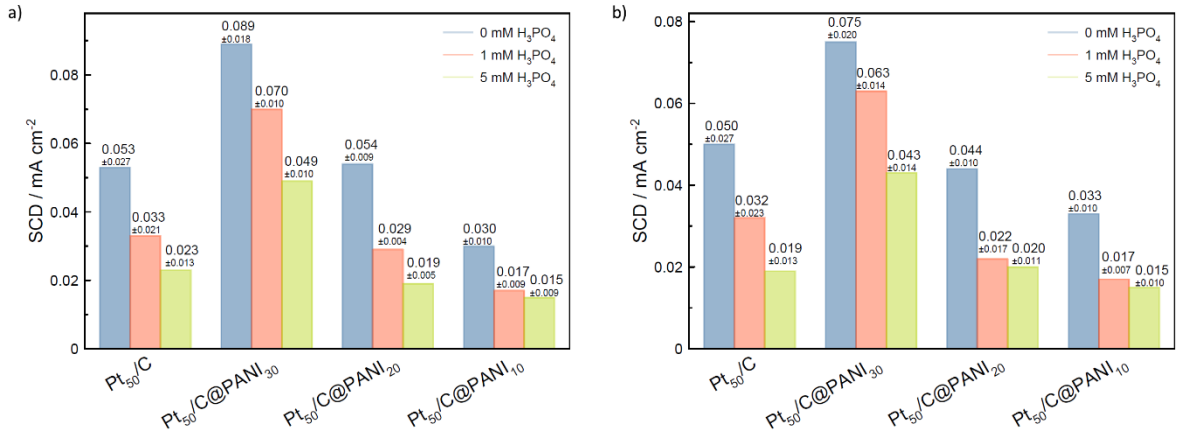

Figure 22 SCD of Pt_{50}/C and Pt_{50}/C@PANI catalysts at a) 1600 rpm and b) at the overall rotation rates (400-2000 rpm) (average of 3 measurements)

In Figure 22 the determined SCD of PANI decorated and undecorated Pt_{50}/C samples of ORR measurements at 1600 rpm and at the overall rotation rates (400-2000 rpm) are illustrated.

As the SCD is a function of A_{active} the results show strongly deviating values. $Pt_{50}/C@PANI_{20}$ and $Pt_{50}/C@PANI_{10}$ feature lower SCD than Pt_{50}/C in pure electrolyte at 1600 rpm. After the addition of PA, their SCD decrease drastically. $Pt_{50}/C@PANI_{30}$ shows the highest SCD of the characterized Pt_{50}/C based catalysts. In pure electrolyte its SCD gives 0.089 ± 0.018 mA cm^{-1}, in 1 mM H_3PO_4 it is calculated to 0.070 ± 0.010 mA cm^{-1}, and in 5 mM H_3PO_4 to 0.049 ± 0.010 mA cm^{-1}, which is both higher than the SCD of the three other catalysts. Moreover, the SCD decreases less dramatically compared to the other samples. However, most importantly, the $Pt_{50}/C@PANI_{30}$ catalyst exhibited better MA and SCD among the four samples in pure electrolyte and when PA was present in the electrolyte.

4.2 $Pt_{20}/@PANI_{30}$ catalyst

As the enhanced stability and improved catalytic activity of the $Pt_{50}/C@PANI_{30}$ is unquestionable, an in-house $Pt_{20}/C@PANI_{30}$ was synthesized by means of the BAE method prior to the functionalization with PANI. CV and ORR measurements of $Pt_{20}/C@PANI_{30}$ and Pt_{20}/C were performed as usual.

4.2.1 Influence of PA on the ECSA of Pt_{20}/C and $Pt_{20}/C@PANI_{30}$ catalysts

The CV of Pt_{20}/C in Figure 23 depicts the typical characteristics of Pt. In the presence of PA the ECSA decreases with increasing H_3PO_4 concentration and Pt-O formation is suppressed by the competitive phosphates adsorption. In contrast, the CV of $Pt_{20}/C@PANI_{30}$, which is illustrated in Figure 24, does not look like a typical CV of Pt. In the region between 0.1 and 0.3 V vs. RHE a smooth H_2 desorption peak is observed instead of distinct peaks related to the Pt surface. However, it is used to determine the ECSA. The double layer region (0.4-0.6 V vs. RHE) looks completely different compared to that of the pure Pt_{20}/C catalyst. The two peaks between 0.4 and 0.8 V vs. RHE are attributed to the oxidation of PANI at positive potentials and to its reduction at negative potentials [34]. Although the original ECSA of $Pt_{20}/C@PANI_{30}$ is lower than that of Pt_{20}/C, the loss of ECSA is reduced, which in turn indicates that phosphates adsorption is inhibited by the PANI film around the catalyst NPs.

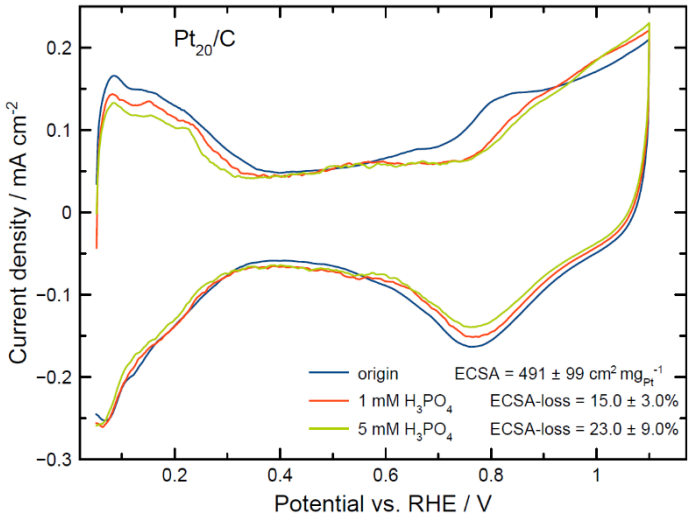

Figure 23 CV curves of Pt_{20}/C catalyst in 0.1 M $HClO_4$ with 0 mM, 1 mM and 5 mM H_3PO_4 (average of 3 measurements)

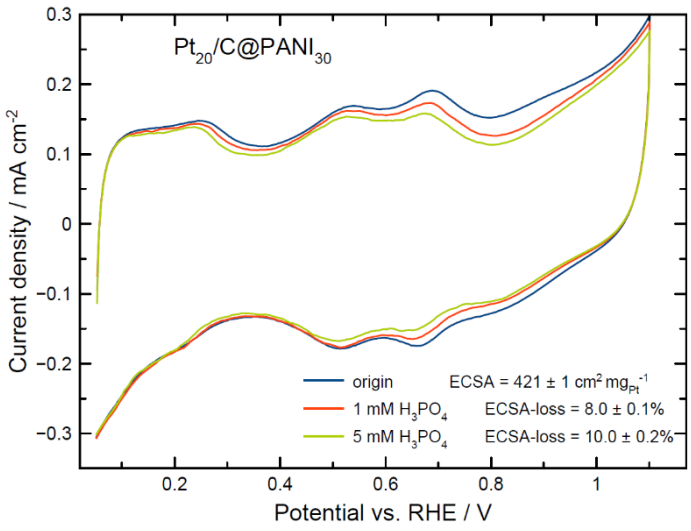

Figure 24 CV curves of Pt_{20}/C@$PANI_{30}$ catalyst in 0.1 M $HClO_4$ with 0 mM, 1 mM and 5 mM H_3PO_4 (average of 3 measurements)

4.2.2 Catalytic activity

Although it was assumed that the PANI content in the Pt_{20}/C@$PANI_{30}$ is too high because of the low value for the origin ECSA, it exhibits improved catalytic activity compared to that of Pt_{20}/C. Figure 25 depicts ORR polarization curves of Pt_{20}/C and Pt_{20}/C@$PANI_{30}$ in pure $HClO_4$ electrolyte as well as in PA containing electrolyte. In 0 mM H_3PO_4 the onset for ORR of Pt_{20}/C@$PANI_{30}$ is distinctly shifted to more positive potentials than that of the Pt_{20}C sample. Latter exhibits less catalytic activity toward ORR in PA containing electrolyte as its onset

potential is shifted to lower potentials. The catalytic activity of Pt_{20}/C decreases faster with increasing acid concentration compared to that of $Pt_{20}/C@PANI_{30}$. This stable behavior of $Pt_{20}/C@PANI_{30}$ confirms again the positive effect of PANI in the catalysts system. The interaction between PANI and the Pt leads to a lower electron density of the functionalized Pt surface, which results in a shift of the d-band center to more positive potentials [8].

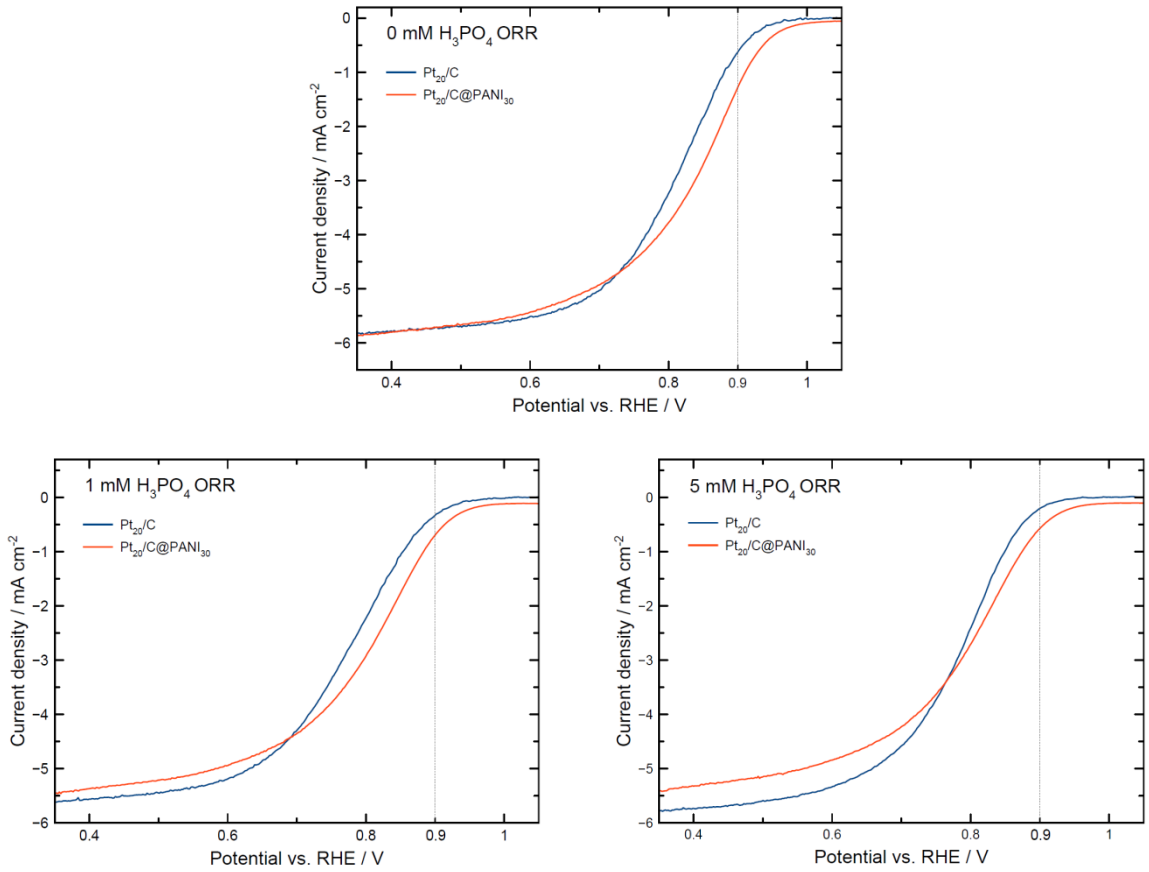

Figure 25 ORR polarization curves of Pt_{20}/C and $Pt_{20}/C@PANI_{30}$ in 0.1 M $HClO_4$ with 0 mM, 1 mM and 5 mM H_3PO_4 at 1600 rpm (average of 3 measurements)

MA and SCD were calculated as described in section 2.4.1. Compared to Pt_{20}/C, $Pt_{20}/C@PANI_{30}$ exhibits a considerable higher MA in pure $HClO_4$ at 1600 rpm, as well as in PA containing electrolyte. $Pt_{20}/C@PANI_{30}$ depicts a MA of 0.039 ± 0.010 A mg^{-1} in $HClO_4$, while the MA of Pt_{20}/C is nearly only half of it. With increasing PA concentration, the MA of both samples decreases, but the MA of $Pt_{20}/C@PANI_{30}$ is still in PA containing electrolyte higher than that

of Pt_{20}/C in pure electrolyte. This is evident from the protecting properties of PANI against phosphate ion adsorption.

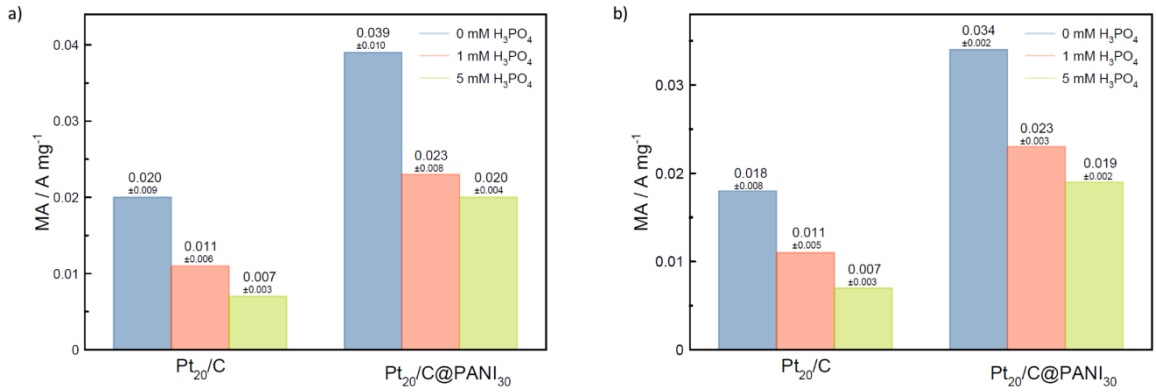

Figure 26 MA of Pt_{20}/C and $Pt_{20}/C@PANI_{30}$ at a) 1600 rpm and b) at the overall rotation rates (400-2000 rpm) (average of 3 measurements)

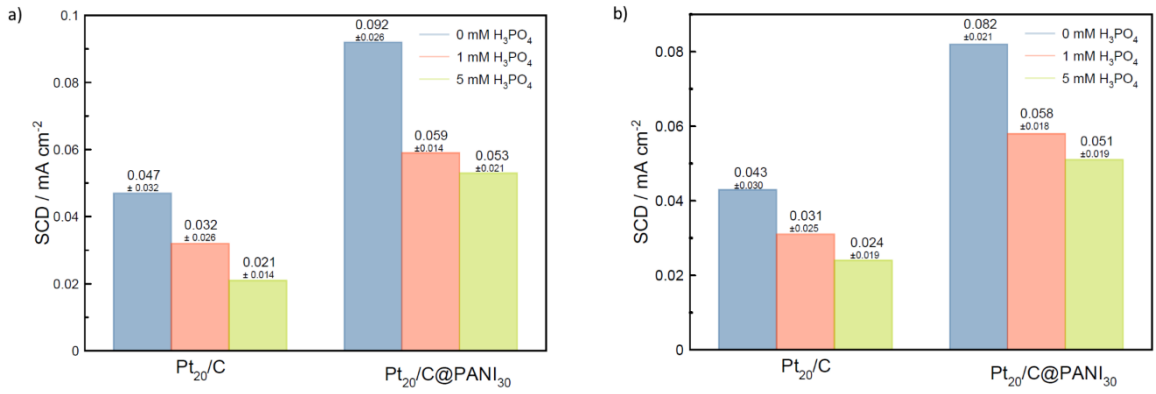

Figure 27 SCD of Pt_{20}/C and $Pt_{20}/C@PANI_{30}$ at a) 1600 rpm and b) at the overall rotation rates (400-2000 rpm) (average of 3 measurements)

The SCD in Figure 27 is much higher for $Pt_{20}/C@PANI_{30}$ than that of pure Pt_{20}/C. As always, the SCD decreases in the presence of PA. But still the lowest SCD of $Pt_{20}/C@PANI_{30}$ (0.053 ± 0.021 mA cm^{-1}) is higher than the SCD of Pt_{20}/C in pure electrolyte (0.047 ± 0.032 mA cm^{-1}) at 1600 rpm. Moreover, by comparing the $Pt_{20}/C@PANI_{30}$ sample with the $Pt_{50}/C@PANI$ samples, the values of its SCD is in the range of the SCD of $Pt_{50}/C@PANI_{30}$, hence higher than Pt_{50}/C, $Pt_{50}/C@PANI_{20}$ and $Pt_{50}/C@PANI_{10}$, although the

content of Pt is lowered. However, Pt_{50}/C@$PANI_{30}$ exhibits the highest MA, followed by Pt_{20}/C@$PANI_{30}$.

4.3 Pt-Co/C@PANI catalysts

It is known, that Pt-Co/C alloys show enhanced catalytic activity in contrast to pure Pt/C catalysts [44]. In addition to Pt_{50}/C@$PANI_{30}$ and Pt_{20}/C@$PANI_{30}$, which pointed out promising results concerning the improved tolerance toward PA, a PANI decorated Pt-Co/C catalyst, which is based on a commercial $Pt_{22.5}$Co/C, was synthesized. Furthermore, via the BAE method an in-house Pt_{15}Co/C was synthesized and then functionalized with PANI. Out of further experiments, a PANI content of 20wt% in Pt-Co/C samples was investigated by CV and ORR measurements as usual.

4.3.1 Influence of PA on the ECSA of Pt-Co/C and Pt-Co/C@ PANI catalysts

The CVs of $Pt_{22.5}$Co/C and $Pt_{22.5}$/C@$PANI_{20}$ are represented in Figure 28 and Figure 29. Both illustrate the typical characteristics of a CV of Pt, such as H_2 adsorption and desorption, the double layer region, Pt-OH and then Pt-O formation as well as Pt reduction. It is evident that the commercial Pt-Co alloy reveals a higher ECSA than the pure Pt_{50}/C. Also, in the presence of PA, its ECSA decreases less strongly than that of the pure Pt catalyst, as phosphates adsorption on the Pt surface could be mitigated by the modification of the electronic structure of Pt by alloying it with late transition metals. These Pt alloys exhibit a d-band center which is down-shifted compared with that of Pt. Thus, adsorption of phosphate ions is weakened [8].

In contrast, the initial ECSA of $Pt_{22.5}$Co/C@$PANI_{20}$ is half as high as that of $Pt_{22.5}$Co/C (see Figure 28 and Figure 29). Therefore, it is assumed that the PANI layer around the catalyst NPs does not favor the interaction between Pt and Co to improve the alloy's catalytic behavior. Unfortunately, the ECSA of $Pt_{22.5}$Co/C@$PANI_{20}$ declines more strongly than the one of $Pt_{22.5}$Co/C after the addition of PA. Usually, considering pure Pt catalysts, the pre-adsorption of PANI groups leads to a decreased availability of three-fold sites on the Pt surface and as a result phosphates adsorption is suppressed ("third-body effect") [8]. Obviously, in the case of $Pt_{22.5}$Co/C@$PANI_{20}$, the PANI groups do not contribute to any inhibition of phosphate species

adsorption. As of now, concerning the Pt-Co alloys, further investigations to optimize the PANI content to inhibit phosphates adsorption need to be done.

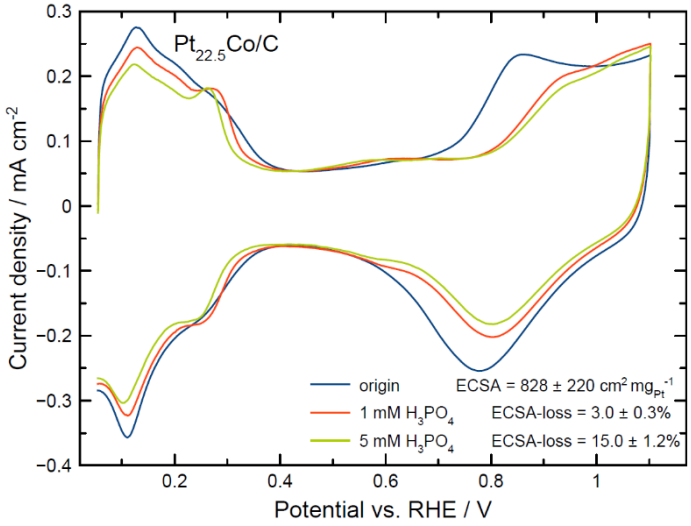

Figure 28 CV curves of $Pt_{22.5}Co/C$ catalyst in 0.1 M $HClO_4$ with 0 mM, 1 mM and 5 mM H_3PO_4 (average of 3 measurements)

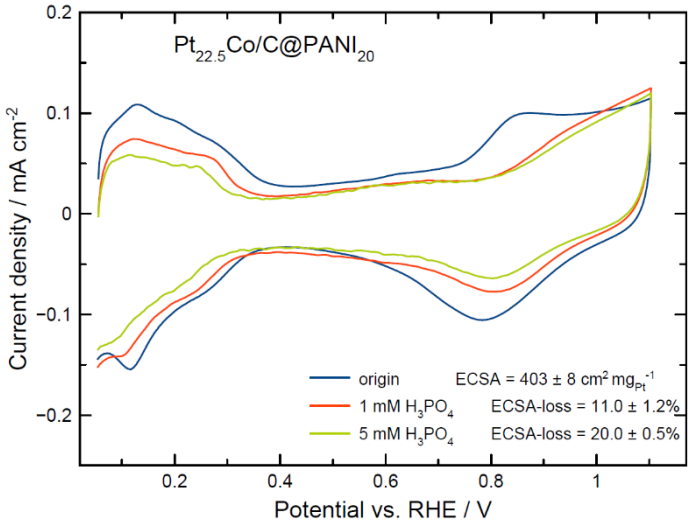

Figure 29 CV curves of $Pt_{22.5}Co/C@PANI_{20}$ catalyst in 0.1 M $HClO_4$ with 0 mM, 1 mM and 5 mM H_3PO_4 (average of 3 measurements)

The CVs of the in-house $Pt_{15}Co/C$ catalyst (Figure 30) exhibit a lower ECSA than that of the commercial $Pt_{22.5}/C$, but a slightly higher ECSA than that of pure Pt/C. This increase in ECSA is mainly due to the post treatment of the catalyst sample. The positive effect of acid-leaching on the performance of Pt-Co/C is attributed to the dissolution of inactive Co and the

separation of Pt on the surface, which leads to an advantageous Pt-skeleton structure. The heat treatment led to the removal of undesired synthesis residues on the catalyst surface [44]. The loss of ECSA in the presence of PA is less dramatic than that of Pt. This is attributed to the mentioned interaction between Pt and Co, which causes weaker phosphates adsorption compared to the pure Pt/C catalyst.

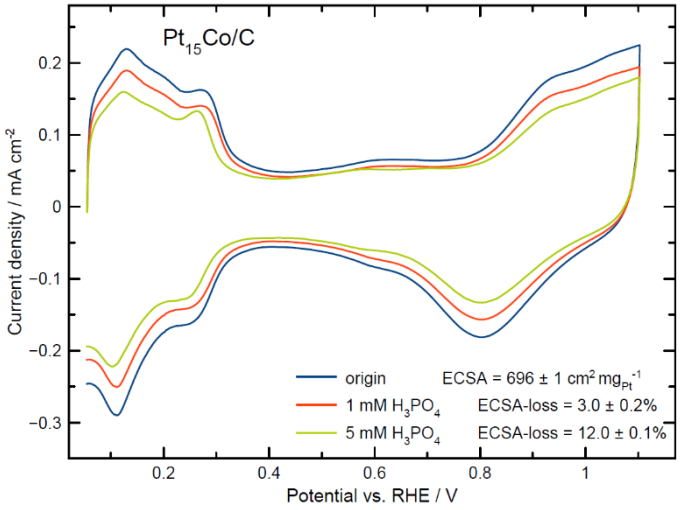

Figure 30 CV curves of $Pt_{15}Co/C$ catalyst in 0.1 M $HClO_4$ with 0 mM, 1 mM and 5 mM H_3PO_4 (average of 3 measurements)

Figure 31 depicts the CV curves of the PANI decorated $Pt_{15}Co/C$ catalyst. Its shape is completely different compared to the other Pt-Co/C samples, but similar to that of the $Pt_{20}/C@PANI_{30}$ catalyst. Neither Pt oxidation, nor Pt reduction could be observed and the H_2 desorption area is very smooth. Latter could be caused by the coverage of the NPs surface by PANI so that the typical peaks referring to the Pt surface are not observable. The peaks in the region between 0.4 and 0.8 V vs. RHE refer to the oxidation and the reduction of PANI [34]. The loss of ECSA in PA containing electrolyte is similar to that of $Pt_{15}Co/C$ and to that of $Pt_{20}/C@PANI_{30}$. This indicates a weaker phosphate ions adsorption due to the alloying of Pt with Co and due to the pre-adsorption of PANI on the catalyst surface.

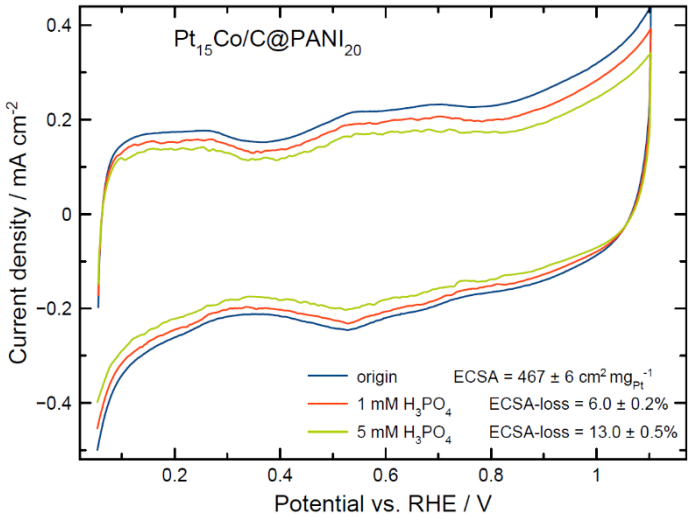

Figure 31 CV curves of $Pt_{15}Co/C@PANI_{20}$ catalyst in 0.1 M $HClO_4$ with 0 mM, 1 mM and 5 mM H_3PO_4 (average of 3 measurements)

4.3.2 Catalytic activity

ORR polarization curves of the Pt-Co/C catalyst samples were recorded in O_2 saturated $HClO_4$ electrolyte with 0 mM, 1 mM and 5 mM H_3PO_4. These are illustrated in Figure 32, where they are compared to Pt_{20}/C as the total metal content is in the same range. In pure electrolyte, the onset potential of the undecorated and PANI decorated Pt-Co/C catalysts is shifted to more positive values than that of Pt_{20}/C. In the presence of PA in the electrolyte, the onset potentials of all four Pt-Co/C samples is shifted to more positive values, but less strongly than that of Pt_{20}/C, and a higher current in the kinetic controlled region is obtained. This indicates the improvement of the catalytic activity as a result of alloying Pt with Co and the formation of a PANI layer to prevent an interaction between the catalyst NPs and PA.

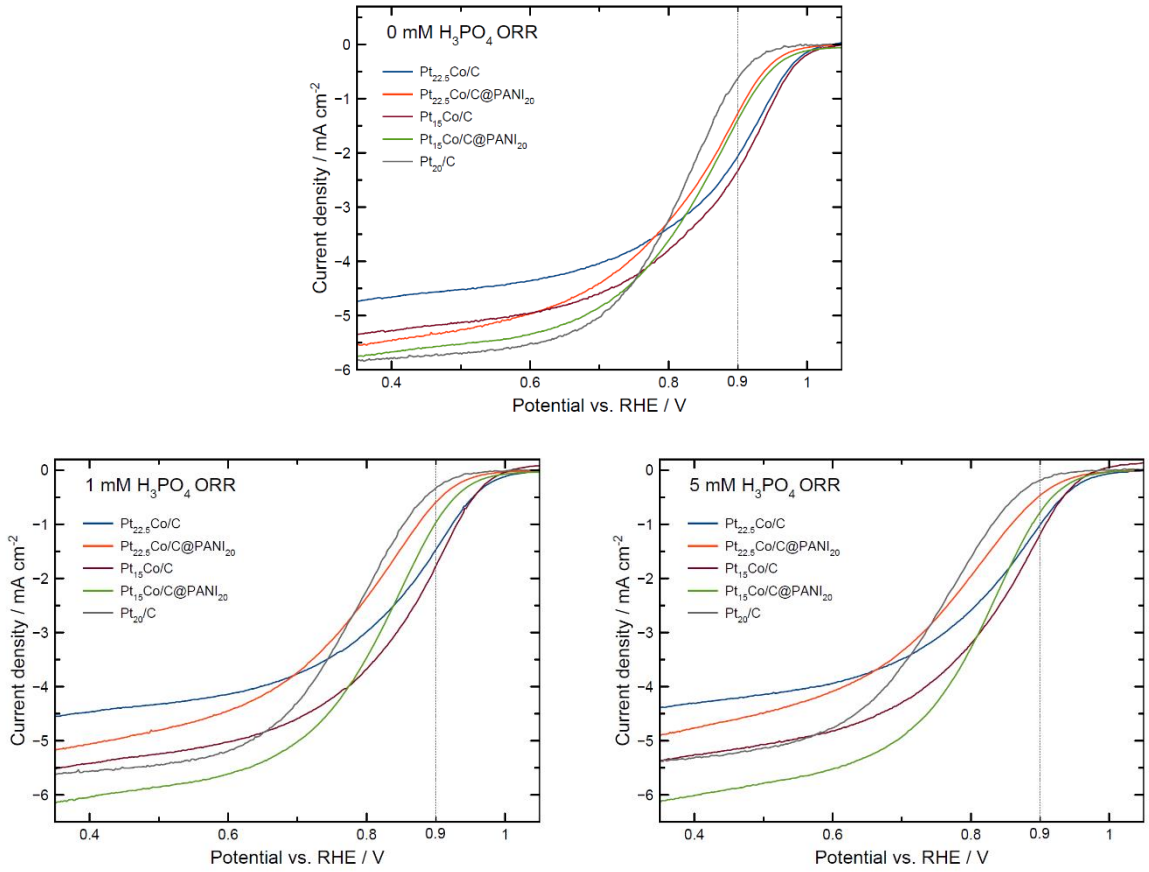

Figure 32 ORR polarization curves of Pt-Co/C and Pt-Co/C@PANI samples in 0.1 M $HClO_4$ with 0 mM, 1 mM and 5 mM H_3PO_4 at 1600 rpm (average of 3 measurements)

The MA of the Pt-Co/C catalyst samples is summarized in Figure 33. Alloying Pt with Co leads to an increase of MA compared to that of Pt_{50}/C. Although $Pt_{15}Co/C$ consists of less Pt than $Pt_{22.5}Co/C$ its MA is higher, even in the presence of PA. This is attributed to the post-treatment of the in-house catalyst sample, which is unknown in the case of the commercial $Pt_{22.5}Co/C$. At 1600 rpm, $Pt_{15}Co/C$ and $Pt_{22.5}Co/C$ show a 2.6-fold increase of MA in pure electrolyte in comparison to the in-house Pt_{20}/C. In 1 mM and 5 mM containing electrolyte their MA is 3.8 and 4.4 times higher than that of Pt_{20}/C. The MA of $Pt_{22.5}Co/C@PANI_{20}$ and $Pt_{15}Co/C@PANI_{20}$ is in fact lower than that of the undecorated samples, but similar to that of the $Pt_{20}/C@PANI_{30}$. Certainly, this could indicate a positive effect of PANI on the Pt-Co alloys.

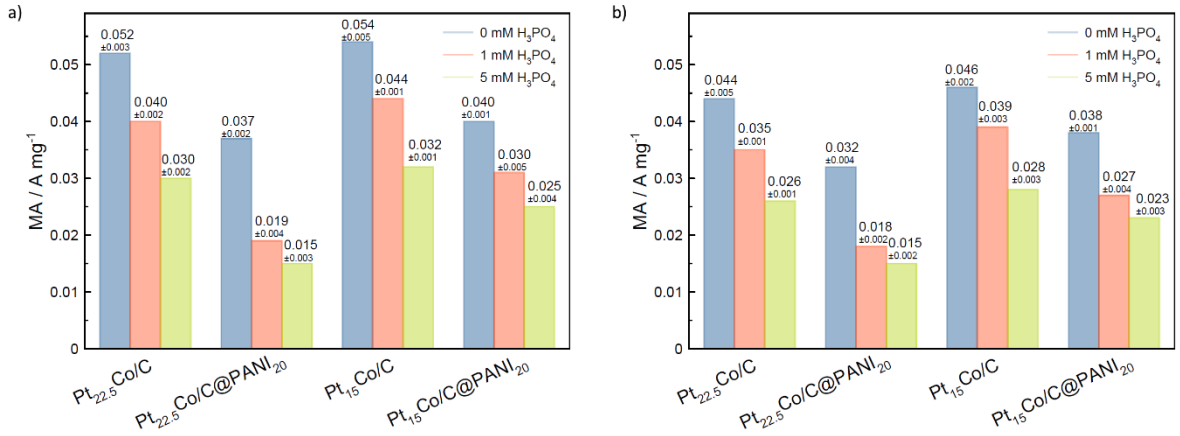

Figure 33 MA of Pt-Co/C and Pt-Co/C@PANI catalysts at a) 1600 rpm and b) at the overall rotation rates (400-2000 rpm) (average of 3 measurements)

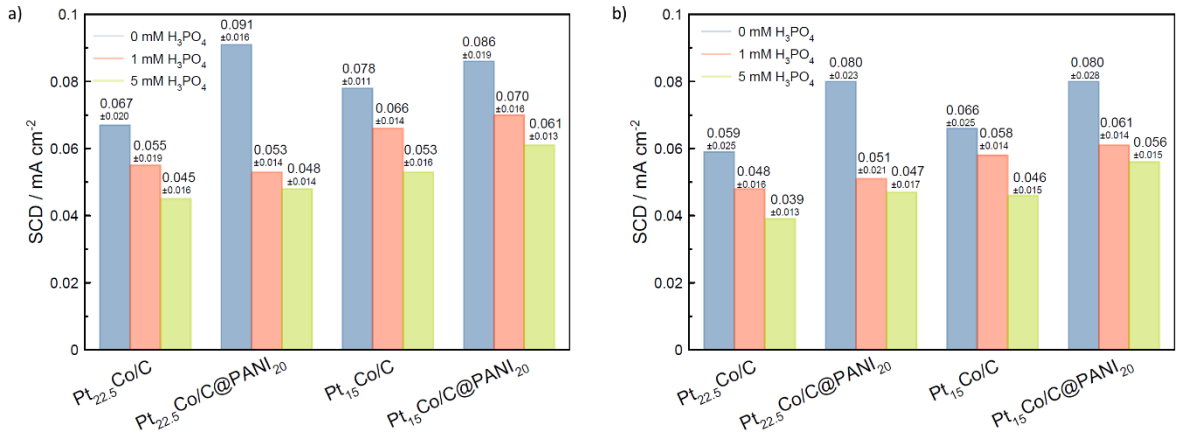

Figure 34 SCD of Pt-Co/C and Pt-Co/C@PANI catalysts at a) 1600 rpm and b) at the overall rotation rates (400-2000 rpm) (average of 3 measurements)

The SCD of the Pt-Co/C and PANI functionalized Pt-Co/C catalysts are represented in Figure 34. At 1600 rpm and at the overall rotation rates (400-2000 rpm), the alloys show an increased SCD in contrast to the Pt/C catalysts in pure electrolyte as well as in PA containing electrolyte. Although the $Pt_{22.5}Co/@PANI_{20}$ and the $Pt_{15}Co/@PANI_{20}$ exhibit lower MA they show a higher SCD than the undecorated alloys due to the low ECSA. Among all catalyst samples their SCD lies in the range of the $Pt_{50}/C@PANI_{30}$ and $Pt_{20}/C@PANI_{30}$, which both demonstrate a positive effect of PANI toward the prevention of phosphates adsorption.

4.4 Levich analysis

The number of electrons, which are involved in the ORR at different rotation rates of the RDE in pure electrolyte and PA containing electrolyte was calculated from the Levich equation (Eq. 13) with the parameters given in the experimental part (section 3.3.1). Plotting the square root of ω against j_d gives a linear relationship with an intersection in the origin.

As shown in Figure 35, Figure 36 and Figure 37 the lines in the Levich plot overlap and are parallel, which indicates that the number of electrons transferred during the ORR remains constant for all catalyst samples, i.e. undecorated and PANI decorated Pt/C and Pt-Co/C samples, and is independent of the PA concentration. So, it becomes apparent, that neither H_3PO_4 nor the PANI content do not change the kinetics of ORR. Approximately always, the ORR followed the favored four electron pathway. If less than four electrons are transferred, not only H_2O but also hydrogen peroxide (H_2O_2) is produced during the reaction of H_2 and O_2.

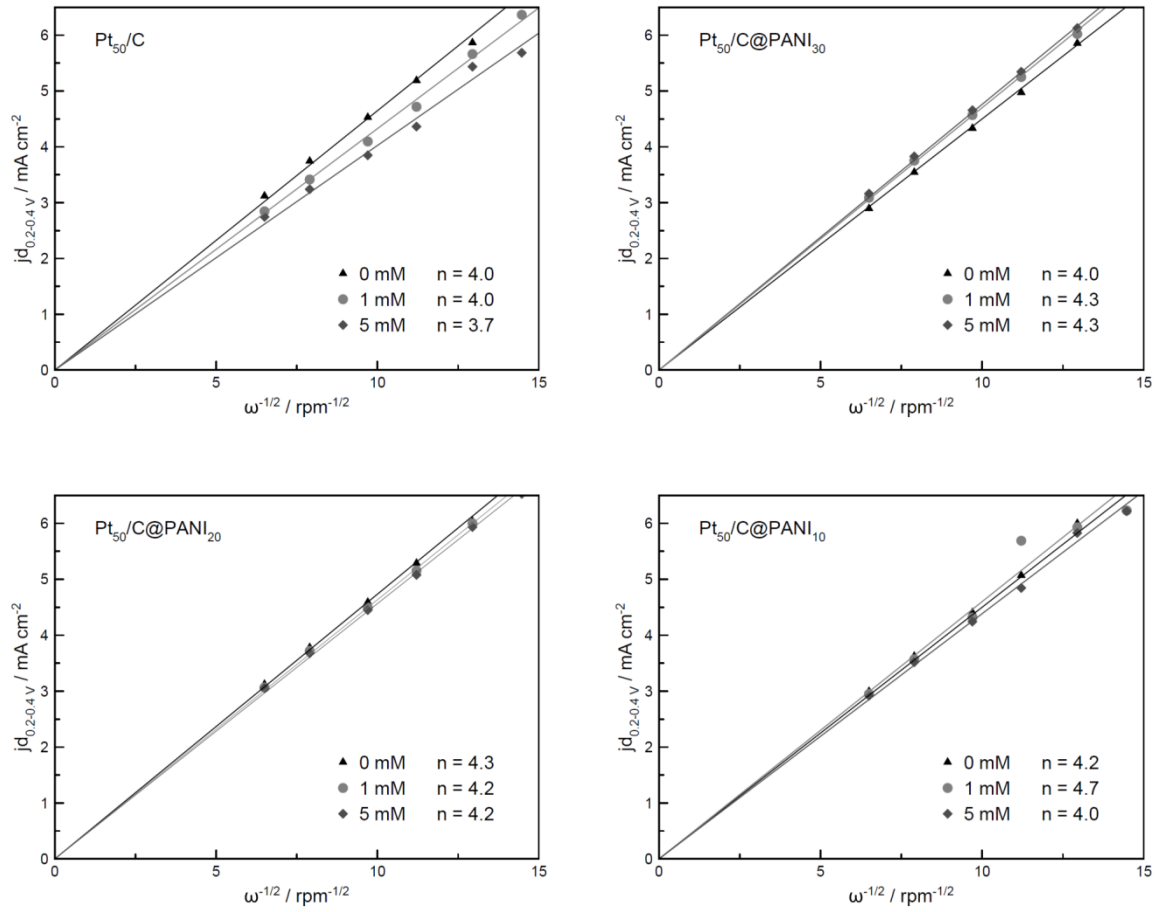

Figure 35 Levich plots of Pt_{50}/C and Pt_{50}/C@PANI catalyst samples (average of 3 measurements)

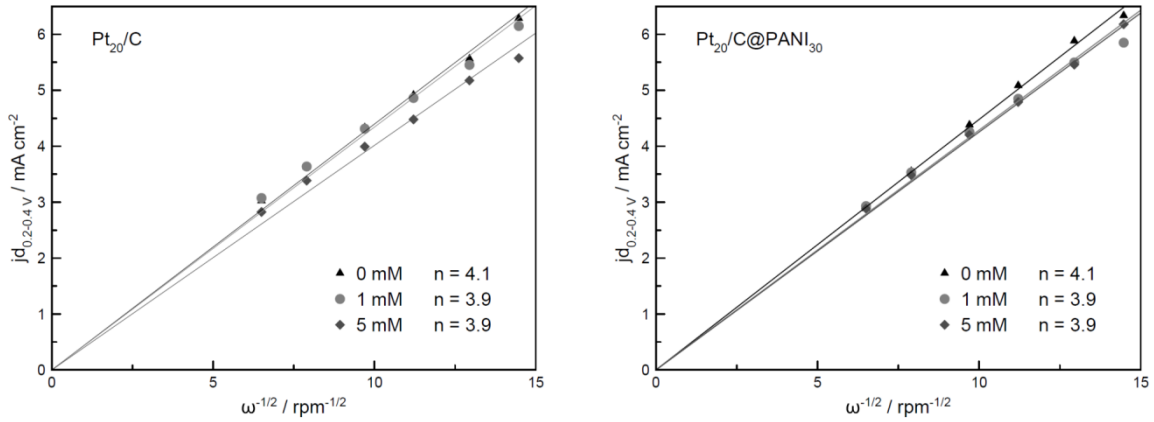

Figure 36 Levich plots of Pt_{20}/C and $Pt_{20}/C@PANI_{30}$ catalyst samples (average of 3 measurements)

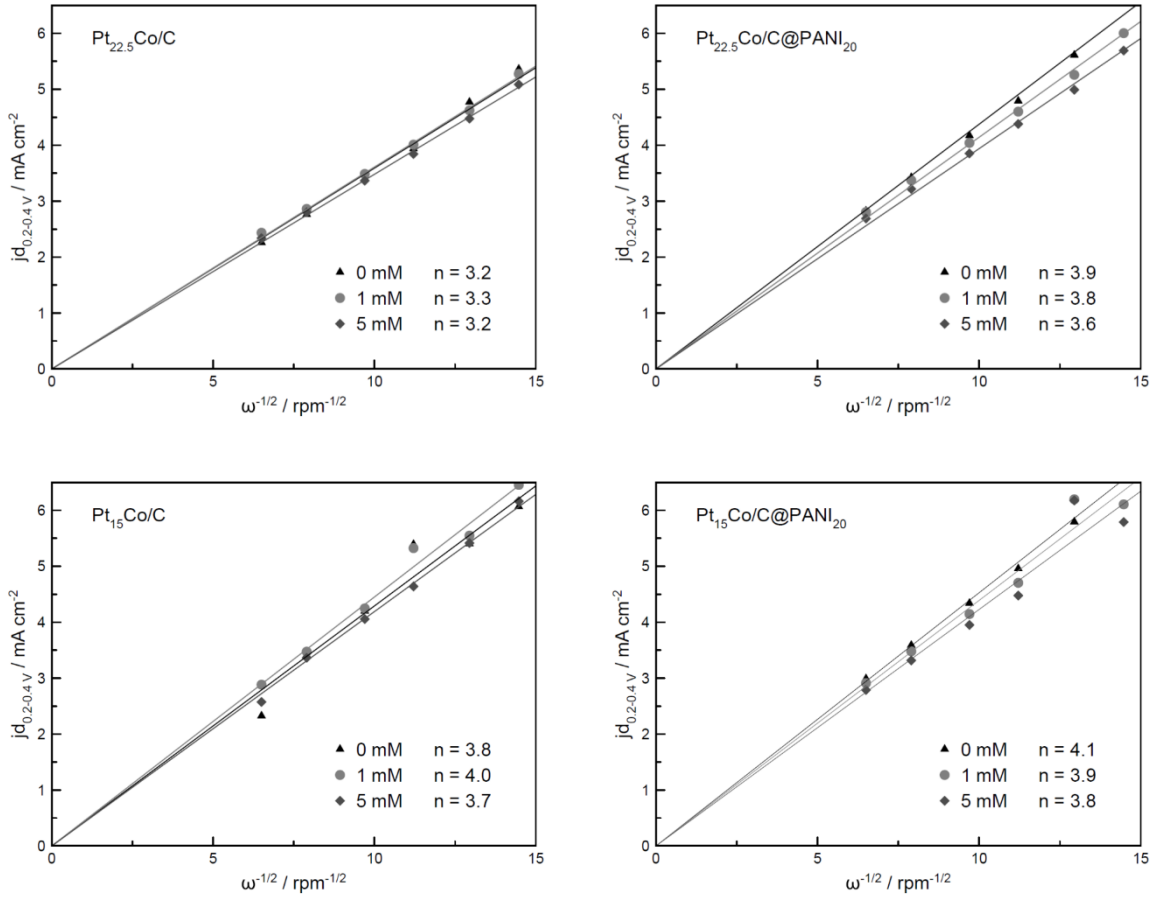

Figure 37 Levich plots of Pt-Co/C and Pt-Co/C@PANI catalyst samples (average of 3 measurements)

5 Summary and outlook

The scope of the present work is to improve the catalytic stability and activity of Pt based cathode catalysts for HT-PEM FCs. Due to presence of PA in the membrane electrolyte of such high temperature FC systems the catalyst performance toward the ORR is limited. Since phosphate species adsorb on the catalyst surface, they inhibit active sites for the catalytic reduction of O_2. In order to mitigate problems associated with PA, functionalization of the catalysts with conducting polymers, such as PANI, have received much attention. Because of its unique properties, PANI prevents the interaction between the Pt surface and PA by forming a thin polymeric film around the catalyst NPs. On the one hand, it protects the carbon support from the corrosive environment and prevents Pt particle agglomeration. On the other hand, an electron delocalization between the Pt d-orbital and PANI changes the electronic structure of the Pt NPs, which favors a weak adsorption of phosphate ions.

In this thesis, with the aim to mitigate phosphates adsorption on the catalyst's catalytic active surface, Pt/C@PANI and Pt-Co/C@PANI catalysts for ORR in HT-PEM FCs were synthesized and electrochemically characterized. The synthesis of PANI decorated commercial Pt/C and Pt-Co/C as well as of in-house Pt/C and Pt-Co/C catalysts followed an oxidative polymerization of aniline. CV and ORR measurements were performed in pure and PA containing (1 mM and 5 mM) 0.1 M $HClO_4$ electrolyte by means of RDE method. Among the prepared catalyst samples the PANI decorated Pt_{50}/C catalysts showed best results concerning stability in pure as well as in PA containing electrolyte. Pt_{50}/C@$PANI_{30}$ showed the highest ECSA in pure electrolyte in comparison to Pt_{50}/C. Also after the addition of PA, the loss of its ECSA amounts only to 1.00 ± 0.02% and 2.00 ± 0.06%, whereas the ECSA of Pt_{50}/C decreased by 21.0 ± 0.3% to 32.0 ± 1.0% in 1 mM and 5 mM H_3PO_4 containing electrolyte, respectively. Pt_{50}/C@$PANI_{20}$ and Pt_{50}/C@$PANI_{10}$ showed indeed a lower initial ECSA than Pt_{50}/C, but PA influences the reduction of their ECSA by only 1.00 ± 0.02% to 15.0 ± 0.3%, which is still lower than the ECSA loss of Pt_{50}/C. Also, Pt_{20}/C@$PANI_{30}$ confirms the positive impact of PANI against phosphates adsorption as its ECSA is reduced less than the one of Pt_{20}/C. $Pt_{22.5}$Co/C and Pt_{15}Co/C revealed an initial ECSA higher than Pt_{50}/C. In the presence of PA, these and the PANI decorated Pt-Co alloys, i.e. $Pt_{22.5}$Co/C@$PANI_{20}$ and Pt_{15}Co/C@$PANI_{20}$, represented a better stability of the ECSA than Pt_{50}/C but not as good as the Pt_{50}/C@$PANI_{30}$ catalyst. Concerning the catalytic activity, at 1600 rpm, Pt_{50}/C@$PANI_{30}$ exhibits a MA which is more than two times higher than that of

Pt_{50}/C in pure electrolyte. In 1 mM and 5 mM H_3PO_4 its MA is around four times higher compared to that of Pt_{50}/C. Also, Pt_{20}/C@$PANI_{30}$ demonstrates a 2- to 3-fold increase of its MA in pure and PA containing electrolyte compared to Pt_{20}/C. Concerning the Pt-Co alloys, $Pt_{22.5}$Co/C and Pt_{15}Co/C represent a higher MA than Pt_{50}/C in pure and PA containing electrolyte. The same is valid for $Pt_{22.5}$Co/C@$PANI_{20}$ and Pt_{15}Co/C@$PANI_{20}$. However, the two latter could not demonstrate higher MA compared to the undecorated equivalents.

In conclusion, the functionalization of Pt based catalyst with PANI was successfully used to prepare new Pt/C@PANI catalysts in which the carbon support is embedded in a PANI shell and the Pt NPs adhere well to the carbon surface. Their improved stability and activity is attributed to the electron interaction between Pt and PANI, which provides the favored inhibition of phosphates adsorption. The experimental results represent that the catalytic stability and activity depend on the thickness of the PANI film, i.e. the PANI content, with respect to the Pt content. Significantly improved stability of Pt_{50}/C@$PANI_{30}$, Pt_{50}/C@$PANI_{20}$ and Pt_{20}/C@$PANI_{30}$ was observed in comparison to the respective undecorated Pt/C catalysts. Considering the catalytic activity, Pt_{50}/C@$PANI_{30}$ and Pt_{20}/C@$PANI_{30}$ exhibit a higher MA than the corresponding Pt/C catalysts in pure and PA containing electrolyte. Also, all undecorated and PANI decorated Pt-Co/C catalysts represent higher MA than both, Pt_{50}/C and Pt_{20}/C, in pure and PA containing electrolyte. Unfortunately, the Pt-Co/C@PANI samples could not demonstrate higher MA in contrast to the Pt-Co/C samples. In any case, Pt_{50}/C@$PANI_{30}$ represents the most promising results in stability and catalytic activity

Future progress would target to identify an appropriate PANI content for Pt-Co alloys with respect to the Pt content in order to avoid phosphates adsorption, hence improve their stability and catalytic activity. Also, the stability and catalytic performance of Pt/C@PANI need to be proved in ex-situ long term measurements. In addition, their catalytic behavior must be investigated when being employed in the MEA.

6 References

[1] U.S. Energy Information Administration, “International Energy Outlook 2016,” 2016.

[2] UNFCCC. Conference of the Parties (COP), “Paris Climate Change Conference-November 2015, COP 21,” 2015.

[3] G. Gahleitner, “Hydrogen from renewable electricity: An international review of power-to-gas pilot plants for stationary applications,” *Int. J. Hydrogen Energy*, vol. 38, pp. 2039–2061, 2013.

[4] U.S. Department of Energy, “Energy Efficiency & Renewable Energy,” 2014.

[5] J. Larminie and A. Dicks, *Fuel Cell Systems Explained*, 2nd ed. Wiley-VCH, 2003.

[6] C. Yang, P. Costamagna, S. Srinivasan, J. Benziger, and A. B. Bocarsly, “Approaches and technical challenges to high temperature operation of proton exchange membrane fuel cells,” *J. Power Sources*, 2001.

[7] S. Kaserer, K. M. Caldwell, D. E. Ramaker, and C. Roth, “Analyzing the Influence of H3PO4 as Catalyst Poison in High Temperature PEM Fuel Cells Using in-operando X-ray Absorption Spectroscopy,” *J. Phys. Chem. C*, vol. 117, no. 12, pp. 6210–6217, 2013.

[8] Y. Li, L. Jiang, S. Wang, and G. Sun, “Influence of phosphoric anions on oxygen reduction reaction activity of platinum , and strategies to inhibit phosphoric anion adsorption,” *Chinese J. Catal.*, vol. 37, no. 7, pp. 1134–1141, 2016.

[9] S. Chen *et al.*, “Nanostructured polyaniline-decorated Pt/C@PANI core-shell catalyst with enhanced durability and activity,” *J. Am. Chem. Soc.*, vol. 134, pp. 13252–13255, 2012.

[10] F. Barbir, “Fuel Cell Electrochemistry,” in *PEM Fuel Cells: Theory and Practice*, 2nd ed., Elsevier Inc., 2013, pp. 33–72.

[11] A. Schenk, “The oxygen reduction reaction in high temperature proton exchange membrane fuel cells: Long term behavior of platinum-cobalt catalysts under ex-situ and in-situ conditions,” TU Graz, 2014.

[12] J. Zhang, J. Wu, H. Zhang, and J. Zhang, “PEM Fuel Cell Fundamentals,” in *Pem Fuel Cell Testing and Diagnosis*, Elsevier B.V., 2013, pp. 1–42.

[13] F. Barbir, “Main Cell Components, Materials Properties and Processes,” in *PEM Fuel Cells: Theory and Practice*, 2nd ed., Elsevier Inc., 2013, pp. 73–113.

[14] A. B. Stambouli, “Fuel cells: The expectations for an environmental-friendly and sustainable source of energy,” *Renew. Sustain. Energy Rev.*, vol. 15, pp. 4507–4520, 2011.

[15] F. Barbir, “Introduction,” in *PEM Fuel Cells: Theory and Practice*, 2nd ed., Elsevier Inc., 2013, pp. 1–16.

[16] F. Barbir, “Fuel Cell Basic Chemistry and Thermodynamics,” in *PEM Fuel Cells: Theory and Practice*, 2nd ed., Elsevier Inc., 2013, pp. 17–32.

[17] H. A. Gasteiger, S. S. Kocha, B. Sompalli, and F. T. Wagner, “Activity benchmarks and requirements for Pt, Pt-alloy, and non-Pt oxygen reduction catalysts for PEMFCs,” *Appl. Catal. B Environ.*, vol. 56, pp. 9–35, 2005.

[18] J. Zhang *et al.*, “High temperature PEM fuel cells,” *J. Power Sources*, vol. 160, pp. 872–891, 2006.

[19] S. S. Araya *et al.*, “A comprehensive review of PBI-based high temperature PEM fuel cells,” *Int. J. Hydrogen Energy*, vol. 41, no. 46, pp. 21310–21344, 2016.

[20] F. Mack, K. Aniol, C. Ellwein, J. Kerres, and R. Zeis, “Novel phosphoric acid-doped PBI-blends as membranes for high-temperature PEM fuel cells.”

[21] J. Zhang, J. Wu, H. Zhang, and J. Zhang, “High-Temperature PEM Fuel Cells,” in *Pem Fuel Cell Testing and Diagnosis*, Elsevier B.V., 2013, pp. 243–282.

[22] J. Rossmeisl, K. S. Gustav, T. Jaramillo, and J. K. Nørskov, “Steady state oxygen reduction and cyclic voltammetry,” *R. Soc. Chem.*, vol. 140, pp. 337–346, 2008.

[23] W. R. Baumgartner *et al.*, “Electrocatalytic Corrosion of Carbon Support in PEMFC at Fuel Starvation,” *ECS Trans.*, vol. 3, no. 1, pp. 811–825, 2006.

[24] M. Bodner, C. Hochenauer, and V. Hacker, “Effect of pinhole location on degradation in polymer electrolyte fuel cells,” *J. Power Sources*, vol. 295, pp. 336–348, 2015.

[25] H. Gregor, *Fuel Cell Technology Handbook*. CRC Press, 2003.

[26] M. Prokop, T. Bystron, M. Paidar, and K. Bouzek, “H3PO3 electrochemical behaviour

on a bulk Pt electrode : adsorption and oxidation kinetics," *Electrochim. Acta*, vol. 212, pp. 465–472, 2016.

[27] J. Lim *et al.*, "Applied Catalysis B : Environmental Oxygen reduction reaction on electrodeposited PtAu alloy catalysts in the presence of phosphoric acid," *"Applied Catal. B, Environ.*, vol. 165, pp. 495–502, 2015.

[28] Q. Li *et al.*, "Phosphate-tolerant oxygen reduction catalysts," *ACS Catal.*, vol. 4, no. 9, pp. 3193–3200, 2014.

[29] Q. Li, J. O. Jensen, R. F. Savinell, and N. J. Bjerrum, "High temperature proton exchange membranes based on polybenzimidazoles for fuel cells," *Prog. Polym. Sci.*, vol. 34, no. 5, pp. 449–477, 2009.

[30] Z. Yin, T. Hu, J. Wang, C. Wang, Z. Liu, and J. Guo, "Preparation of highly active and stable polyaniline-cobalt-carbon nanotube electrocatalyst for oxygen reduction reaction in polymer electrolyte membrane fuel cell," *Electrochim. Acta*, vol. 119, pp. 144–154, 2014.

[31] A. J. Medford *et al.*, "From the Sabatier principle to a predictive theory of transition-metal heterogeneous catalysis," *J. Catal.*, vol. 328, pp. 36–42, 2015.

[32] I. Katsounaros, S. Cherevko, A. R. Zeradjanin, and K. J. J. Mayrhofer, "Oxygen electrochemistry as a cornerstone for sustainable energy conversion," *Angew. Chemie - Int. Ed.*, vol. 53, pp. 102–121, 2014.

[33] I. E. L. Stephens, A. S. Bondarenko, U. Grønbjerg, and I. Chorkendorff, "Understanding the electrocatalysis of oxygen reduction on platinum and its alloys," *Energy Environ. Sci.*, vol. 5, pp. 6744–6762, 2012.

[34] Z. Yin, T. Hu, J. Wang, C. Wang, Z. Liu, and J. Guo, "Electrochimica Acta Preparation of highly active and stable polyaniline-cobalt-carbon nanotube electrocatalyst for oxygen reduction reaction in polymer electrolyte membrane fuel cell," *Electrochim. Acta*, vol. 119, pp. 144–154, 2014.

[35] S. M. Reda and S. M. Al-Ghannam, "Synthesis and Electrical Properties of Polyaniline Composite with Silver Nanoparticles," *Adv. Mater. Phys. Chem.*, vol. 2, no. 2, pp. 75–81, 2012.

[36] Z. A. Boeva and V. G. Sergeyev, “Polyaniline: Synthesis, properties, and application,” *Polym. Sci. Ser. C*, vol. 56, no. 1, pp. 144–153, 2014.

[37] Z. Durmus, A. Baykal, H. Kavas, and H. Sözeri, “Preparation and characterization of polyaniline (PANI)–Mn3O4 nanocomposite,” *Phys. B Condens. Matter*, vol. 406, no. 5, pp. 1114–1120, 2011.

[38] X. Sun, N. Zhang, and X. Huang, “Polyaniline-Coated Platinum Nanocube Assemblies as Enhanced Methanol Oxidation Electrocatalysts,” *ChemCatChem*, vol. 8, no. 22, pp. 3436–3440, 2016.

[39] L. Li, L. Hu, J. Li, and Z. Wei, “Enhanced stability of Pt nanoparticle electrocatalysts for fuel cells,” *Nano Res.*, vol. 8, no. 2, pp. 418–440, 2015.

[40] K. J. J. Mayrhofer, D. Strmcnik, B. B. Blizanac, V. Stamenkovic, M. Arenz, and N. M. Markovic, “Measurement of oxygen reduction activities via the rotating disc electrode method : From Pt model surfaces to carbon-supported high surface area catalysts,” vol. 53, pp. 3181–3188, 2008.

[41] Y. Garsany, O. A. Baturina, K. E. Swider-Lyons, and S. S. Kocha, “Experimental methods for quantifying the activity of platinum electrocatalysts for the oxygen reduction reaction,” in *Analytical Chemistry*, 2010.

[42] S. Chen *et al.*, “Supporting Information Nanostructured Polyaniline-Decorated Pt/C@PANI Core – Shell Catalyst with Enhanced Durability and Activity,” pp. 1–12, 2012.

[43] Y. Holade, K. Servat, J. Rousseau, C. Canaff, and S. Poulin, “Electrochemical and Physicochemical Characterizations of Gold-Based Nanomaterials : Correlation between Surface Composition and Electrocatalytic Activity,” vol. 162, no. 14, 2015.

[44] A. Schenk *et al.*, “Platinum-cobalt catalysts for the oxygen reduction reaction in high temperature proton exchange membrane fuel cells e Long term behavior under ex-situ and in-situ conditions,” *J. Power Sources*, vol. 266, pp. 313–322, 2014.

7 Appendix

7.1 List of figures

7.2 List of tables